JGR Atmospheres

RESEARCH ARTICLE
10.1029/2020JD032825

First Observations of Elves and Their Causative Very Strong Lightning Discharges in an Unusual Small-Scale Continental Spring-Time Thunderstorm

Ivana Kolmašová[1,2], Ondřej Santolík[1,2], Petr Kašpar[1], Martin Popek[1], Andrea Pizzuti[3,4], Pavel Spurný[5], Jiří Borovička[5], Janusz Mlynarczyk[6], Jyrki Manninen[7], Edith L. Macotela[7], Petr Zacharov[8], Radek Lán[1], Luděk Uhlíř[1], Gerhard Diendorfer[9], Alec Bennett[3,4], Martin Füllekrug[3], and Rudolf Slošiar[10]

[1]Department of Space Physics, Institute of Atmospheric Physics, Czech Academy of Sciences, Prague, Czech Republic, [2]Faculty of Mathematics and Physics, Charles University, Prague, Czech Republic, [3]Department of Electronic and Electrical Engineering, University of Bath, Bath, UK, [4]Bristol Industrial and Research Associates Limited, Bristol, UK, [5]Interplanetary Matter Department, Astronomical Institute, Czech Academy of Sciences, Ondrejov, Czech Republic, [6]Department of Electronics, AGH University of Science and Technology, Krakow, Poland, [7]Sodankylä Geophysical Observatory, Sodankylä, Finland, [8]Department of Meteorology, Institute of Atmospheric Physics, Czech Academy of Sciences, Prague, Czech Republic, [9]Department of ALDIS, OVE Service GmbH, Vienna, Austria, [10]SOSA (Slovak Organization for Space Activities), Bratislava, Slovakia

Key Points:

- Observed elves were produced during a small-scale continental spring-time thunderstorm
- The fraction of intense positive cloud-to ground lightning strokes reached 55%
- Only very strong strokes (> ~300 kA) were capable to excite observable elves during this thunderstorm

Correspondence to:
I. Kolmašová,
iko@ufa.cas.cz

Citation:
Kolmašová, I., Santolík, O., Kašpar, P., Popek, M., Pizzuti, A., Spurný, P., et al. (2021). First observations of elves and their causative very strong lightning discharges in an unusual small-scale continental spring-time thunderstorm. *Journal of Geophysical Research: Atmospheres*, *126*, e2020JD032825. https://doi.org/10.1029/2020JD032825

Received 28 MAR 2020
Accepted 25 NOV 2020

Abstract We show for the first time that elves can be produced by an unusual small-scale continental spring-time thunderstorm. The storm occurred in Central Europe, covered a very small area of ~50 × ~30 km and lasted only for ~4 h on April 2, 2017. The fraction of intense positive cloud-to-ground lightning strokes was unusually high, reaching 55%, with a mean peak current of 64 kA. The peak currents of return strokes (RS) associated with elves exceeded ~300 kA. Elves and their causative RS have been observed with different optical and electromagnetic recordings. Signatures of ionospheric disturbances indicating the presence of elves were found in measurements of displacement currents, ionospheric reflections of sferics and man-made narrow-band transmissions. All these electromagnetic observations coincide with four optical detections of elves and strongly suggest the occurrence of two more elves later in the decaying phase of the storm. Surprisingly, the same electromagnetic measurements indicate that other strong strokes did not produce any elves. Our simulation results show that the formation of an elve is not only determined by the high-peak current of their causative strokes but that it is also controlled by the conductivity of the lightning channels and velocity of the current wavefront. We hypothesize that because of a lower conductivity of RS lightning channels and/or slower current waves only very strong strokes with peak currents above ~300 kA might have been capable to produce observable elves during this thunderstorm.

1. Introduction

Elves are short-lived (<1 ms) transient luminous events (TLEs) which have been detected by low light cameras in the visible wavelength range at altitudes of about ~90 km just after the onset of cloud-to-ground (CG) lightning discharges (Fukunishi et al., 1996; Inan et al., 1996). An elve has the shape of a narrow expanding ring propagating outwards from its central position above the parent lightning to horizontal distances up to ~50–350 km (Barrington-Leigh & Inan, 1999; Fukunishi et al., 1996). The optical luminosity of elves originates in the heating of ionospheric electrons and the subsequent excitation and ionization of N_2 molecules in the lower ionosphere by an intense electromagnetic pulse from a strong CG lightning discharge (Inan et al., 1997). Elves can be produced by lightning discharges of both positive and negative polarities (Barrington-Leigh & Inan, 1999). Marshall et al. (2015) reported exceptional observations of elves produced by intracloud (IC) lightning strokes, forming doublets with the reflection of the electromagnetic waves from the ground. Elve doublets could also occur after a class of terrestrial gamma ray flash events as shown theoretically by Liu et al. (2017). This was very recently confirmed experimentally by Neubert et al. (2019) using Atmosphere-Space Interactions Monitor onboard the International Space Station. Tiger elves with a striped luminosity modulated by convectively generated gravity waves (Moudry et al., 2003; van der Velde et al., 2011; Yue & Lyons, 2015) have also been exceptionally observed. Recently, Mussa

et al. (2019) reported observations of elves by the fluorescence detectors of the Auger Observatory, which are now equipped with an innovative trigger developed for the detection of elves.

Simulations of optical emissions of elves with a typical donut shape are consistent with observations (Barrington-Leigh & Inan, 1999; Cho & Rycroft, 1998; Inan et al., 1991, 1996; Kuo et al., 2007; Marshall et al., 2010; Taranenko et al., 1993; Veronis et al., 1999). The hole radius of elves is believed to be related to velocities of return stroke current wave (Blaes & Inan, 2014). They found that with a confidence of 95% the causative RS current waves traveled between 52% and 94% of the speed of light. On the other hand, typical velocities of the current wave in positive lightning RS channels reach only one third of the speed of light (Mach & Rust, 1993). Kuo et al. (2012) developed a full kinetic model of elves with a wide spectral range from UV, visible to near-infrared wavelengths. They showed that the first positive band of nitrogen represented a major emission band. Pérez-Invernon et al. (2018a, 2018b) introduced recently a new model of elves which includes calculations of the temporal evolution of more than 130 species in the lower ionosphere interacting through >1,000 elementary processes to estimate optical spectra of elves. They did not find any differences in spectral characteristics of elves associated with energetic CG or IC discharges.

First estimates of the lower limit of the peak current for lightning strokes that produce elves were published by Newsome and Inan (2010). According to their results, elves are produced with a cumulative probability of reaching 50% at a peak current of 120 kA. However, subsequent observations showed different values. For example, based on photometer measurements and very low frequency (VLF) electromagnetic wave recordings conducted in the western US, Blaes et al. (2016) predicted that the cumulative probability of 50% to produce elves would be reached already for CG return strokes (RS) with peak currents of 88 kA. Using recordings with the Imager of Sprites and Upper Atmospheric Lightning (ISUAL) on board the FORMOSAT2 satellite and corresponding World Wide Lightning Location Network data, A. B. C. Chen et al. (2014) estimated a lower limit of peak currents ∼38 kA, to generate elves. However, van der Velde and Montanyà (2016) found a lower limit of the peak current to be close to 130 kA for strokes that produced elves in northeastern Spain. Note, that the sensitivity of optical sensors and background luminosity level of the sky might play a role in the determination of the peak current limit for elves detection (A. B. Chen et al., 2008). Moreover, the peak current is not the only parameter driving the generation of elves; it is also influenced by the background neutral density, the electron density at the altitude of elves, and also by parameters of RS processes other than the peak current. Electromagnetic signals emitted by the causative lightning strokes in the VLF and extremely low frequency (ELF) ranges can propagate thousands of kilometers in the Earth-ionosphere waveguide. Therefore, their analysis serves as an ideal tool for studying elves-producing lightning. The properties of the parent lightning strokes producing elves, such as the polarity, current moment, and charge moment can be determined with broadband VLF and ELF measurements (Barrington-Leigh & Inan, 1999; Cummer, 2003; Haldoupis et al., 2013; Inan et al., 2010 and references herein; Mlynarczyk et al., 2015). Huang et al. (1999) investigated Schumann resonances excited by sprite and elves producing strokes. They clearly showed that charge moment changes derived from ELF measurements are larger for sprites generating strokes in spite of the fact that peak currents in the elves lightning events typically exceed those associated with sprite. They also did not find any relation between peak currents and charge moment change values for elves producing strokes.

Changes of ionization caused by elves are also observed as perturbations of the subionospheric propagation of narrowband VLF signals emitted by powerful transmitters dedicated to the communication with submarines (Haldoupis et al., 2004, 2013; Mika et al., 2006). This phenomenon is known as a long-recovery early event (LORE) since after an impact of a strong lightning stroke of any polarity (>250 kA) the electron density in the lower ionosphere does not recover for many minutes. The probability of detections of LORE perturbations approaches unity for discharges stronger than 300 kA if located within ∼250 km from the great circle path of a VLF transmitter-receiver link (Haldoupis et al., 2013). The LORE phenomenon is considered as a VLF fingerprint of elves. Farges et al. (2007) observed a strong and very brief attenuation of narrowband broadcasting signals (500–1,600 kHz) just after strong CG lightning discharges of both polarities. They showed that this effect was due to electron heating in the lower ionosphere. Such perturbation might be considered as a signature of elves in the medium frequency range.

Novel quasistatic electric field measurements detect lightning activity up to a range of ∼100 km from the detector (Bennett & Harrison, 2013). The source of these signals is a charge neutralization by lightning,

which has usually a relatively small horizontal extent. Nevertheless, these detectors are able to record signals from TLE located up to ~1,000 km away due to horizontally extensive lower ionospheric electron density enhancements. This effect was observed to be associated with sprites (Füllekrug et al., 2013) or halos (Bennett, 2014). However, it was never reported to be associated with elves.

Elves-producing thunderstorms differ in both size and structure from ordinary thunderstorms. During the summer, elves predominantly appear above well-developed stratiform regions of mesoscale convection systems with large reservoirs of positive charge. The storm area usually exceeds ~2.10^4–25.10^4 km^2 and typically reaches ~10^5 km^2 (Soula et al., 2009). Such systems can develop above both landmasses and oceans. The observations of the ISUAL satellite (A. B. C. Chen et al., 2014) showed that in summer the most active elves-producing storms appeared on the western coastal area of the Northern America, in the equatorial Africa, and the equatorial Southeast Asia. In winter, thunderclouds develop in a colder atmosphere, tend to cover smaller areas, and cloud-tops are lower. In Japan, strong CG discharges with a large charge moment were found to take place near the convective core of winter thunderclouds (Figure 7 in Takahashi et al., 2003). As elves are produced by electromagnetic pulses generated by high peak current lightning strokes of any polarity, winter thunderclouds are more favorable for the production of elves having stronger charge centers and larger electric fields (van der Velde & Montanyà, 2016). As far as reported in the literature concerning the northern hemisphere elve-producing winter thunderstorms, such were exclusively observed in the coastal region of Japan (Hobara et al., 2001; Suzuki et al., 2011; Takahashi et al., 2003), in the Mediterranean region (Greenberg et al., 2007; Montanyà et al., 2010; Yair et al., 2009), and over the Bay of Biscay (van der Velde & Montanyà, 2016). The occurrence of elves in the area of the Bay of Biscay is not surprising, as the thunderstorms in this region were found to produce superbolts with energies above 2 MJ (Holzworth et al., 2019). The majority of 800 elves recorded by a low-light camera in north-eastern Spain and reported by van der Velde and Montanyà (2016) occurred above the Atlantic maritime thunderstorms.

In this study, we present the first observation of a small-scale continental spring-time thunderstorm producing elves. We analyze elves and their causative lightning strokes which occurred in the southwest of Czechia and which have been simultaneously recorded by different observational techniques on April 2, 2017. We combine optical and electromagnetic measurements with a focus on positive lightning discharges with high peak currents >100 kA. We observe an extremely large lower limit ~300 kA for the peak current of elve-producing strokes and we compare the properties of discharges, which produced elves with those for which elves were not detected. We use our observations as an input for an elve inception model to determine additional parameters of the return stroke that lead to elve production. In Sections 2 and 3, we describe the meteorology of the thunderstorm and our instrumental setup. In Section 4, we analyze and discuss different, simultaneously conducted optical and electromagnetic records of elves, their causative lightning strokes and other strong strokes occurring in the same thunderstorm. In Section 5, we introduce our elve inception model to simulate optical emissions in the lower ionosphere related to return stroke currents >100 kA, and in Section 6, we summarize our results.

2. Thunderstorm on April 2, 2017

A large low-pressure trough with the axis extending from Scandinavia to northern Italy traveled slowly eastward and created favorable conditions for deep moist convection, especially on its eastern side. Organized convective storms occurred over Germany and neighboring countries, where moderate convective available potential energy (CAPE) overlapped with a weak to moderate vertical wind shear. According to the radar measurements from the Czech radar network operated by the Czech Hydrometeorological Institute (Novák, 2007) the storm formed ~16:00 UTC in Germany close to the Czech border and moved across the Bohemian Forest to Czechia. The storm decayed at around 23:00 UTC. In the vicinity of the storm, there has been a CAPE of 375 J/kg and a weak deep-layer shear of around 10 m/s measured at the Kümmersbruck sounding station, Germany (49.4°N, 11.9°E) at 18:00 UTC. Storms are very rare in this region in April, which is consistent with results of Taszarek et al. (2018) who did not find the CAPE values above 100 J/kg during this month in Central Europe. On the other hand, the observed value of 375 J/kg is below the average for the summer season. The storm had a multicell character and covered a very small area of about 1,500 km^2. Based on radar measurements, the cloud height and cloud-top temperature were estimated to 9.5 km and −51°C, respectively. The global maps for the winter and summer seasons published by Wilcox

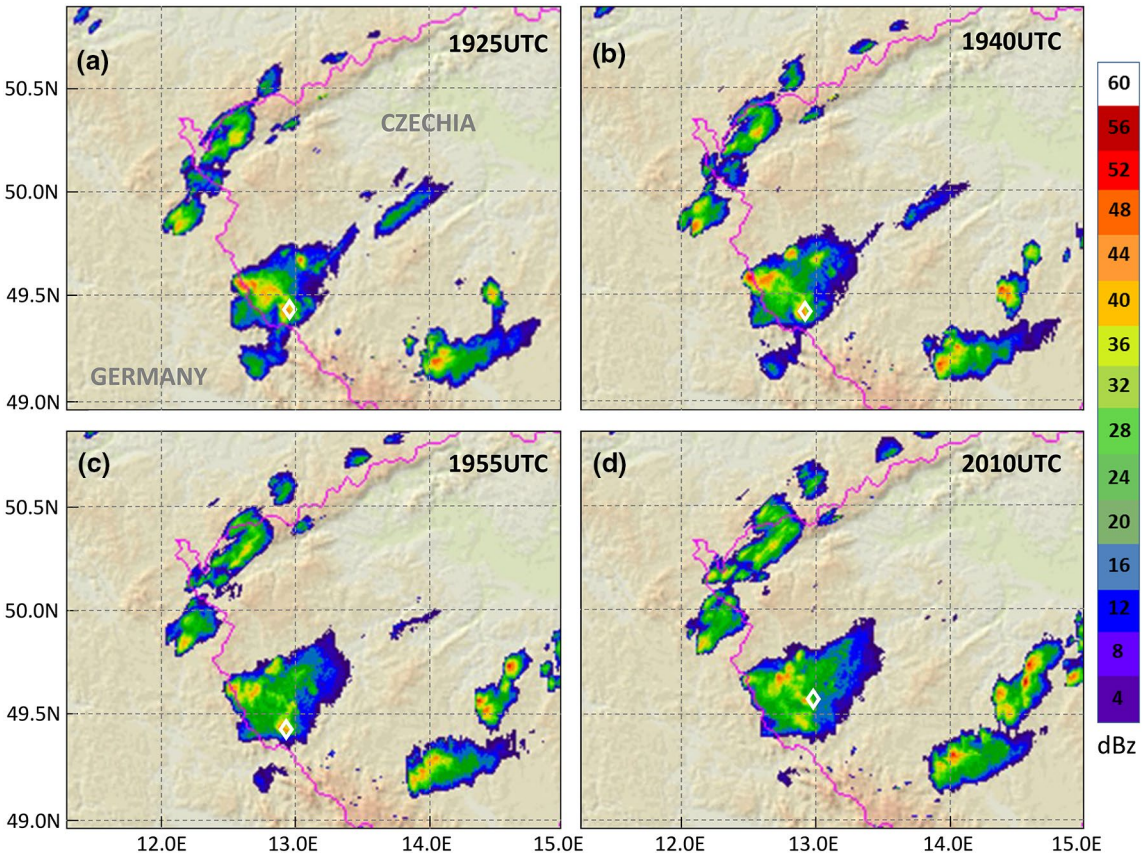

Figure 1. Weather radar plots from April 2, 2017 provided by the Czech radar network consisting of two polarimetric Doppler weather radars Skalky and Brdy (Vaisala WRM-200) operated by the Czech Hydrometeorological Institute. Times (in UTC) of plots a–d are chosen to be the closest to optical observation of elves E1–E4. Locations (represented by white diamonds) and times of occurrence of causative strokes were provided by the lightning detection network European Cooperation for Lightning Detection (EUCLID). The magenta line represents the western border of Czechia.

et al. (2012) placed the territory of Czechia in the interval of tropopause heights from 9.5 to 11 km in both seasons and tropopause temperatures were between −60°C and −55°C (winter) or from −55°C to −50°C (summer). The measured cloud height of this spring-time thunderstorm is therefore consistent with the lower bound of the Wilcox et al. (2012) tropopause height interval, suggesting the similarity to the situation in winter, while the measured cloud-top temperature falls in the summer-time interval of tropopause temperatures. This unusual spring-time thunderstorm therefore has meteorological properties of both winter and summer events. The meteorological radar plots closest to the occurrence times of the observed elves indicate that the causative RS (represented by white diamonds in Figure 1) were predominantly located in the high radar reflectivity areas indicated by the red color. The ground air temperature measured at the closest meteorological station (Domažlice, Czechia, 49.4°N, 12.9°E) reached an unusually high value of 24°C during the afternoon hours. The daily average temperature on April 2 was 17°C, about 11°C larger than its typical value derived from long-term observations.

3. Instrumentation

The locations of the various instruments used in this study are shown in Figure 2. A TLE observing site of the Department of Space Physics at the Institute of Atmospheric Physics of the Czech Academy of Sciences is located in Nydek, Czechia (49.7°N, 18.8°E) at a distance of 430 km from the thunderstorm. Video frames of three Watec 910HX cameras were recorded with a resolution of 720 × 576 pixels. Twenty-five video frames were recorded every second such that the effective time resolution is 40 ms. Focal lengths of lenses in all three cameras were the same (10 mm) and their effective horizontal field of view was 37°. Two cameras

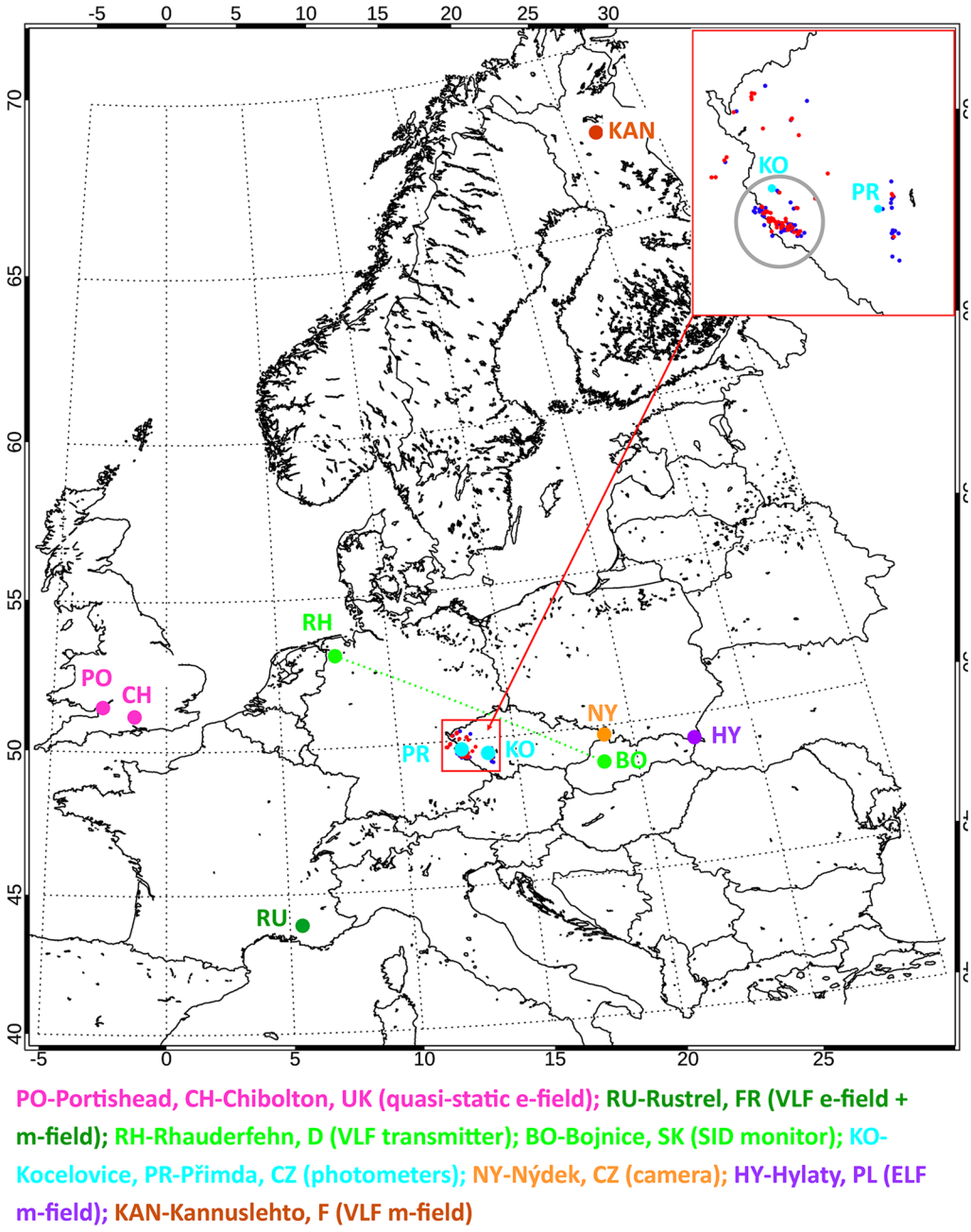

Figure 2. Location of the elve-producing thunderstorm is marked by a gray circle in the inset on the top right-hand side. Positions of all positive and negative CG lightning discharges detected by EUCLID during the analyzed thunderstorm (18:30–22:30 UTC) are represented by red and blue dots, respectively, in an area restricted to latitudes ranging from 49.0°N to 50.5°N and longitudes from 12.0°E to 14.0°E. Locations of individual instruments are represented by colored dots.

are equipped with a GPS video time inserter, which provide information on the start and end times of the exposure time for each video frame. The UFOCapture V2 event detection and analyzer software package (http://sonotaco.com/) is used to record transient optical phenomena and to process the records.

High-speed photometers installed in the Digital Autonomous Fireball Observatory measuring units have been deployed by the Astronomical Institute of the Czech Academy of Sciences at 14 places in Czechia in scope of the European fireball network (Spurný et al., 2017). These all-sky photometers record high-reso-

lution radiometric light curve profiles with a sampling frequency of 5 kHz and/or 500 Hz. The system time is controlled by the PPS pulse of the GPS signal. We have used data from Czech stations Přimda (12.7°N, 49.7°E) and Kocelovice (13.8°N, 49.5°E), which were located at a distance of 20 and 100 km from the investigated thunderstorm, respectively.

A three-component VLF receiving station of the Department of Space Physics, Institute of Atmospheric Physics of the Czech Academy of Sciences is placed at the external measurement site of the Laboratoire Souterrain à Bas Bruit on the summit of La Grande Montagne (43.9°N, 5.5°E) close to Rustrel, France at a distance of 820 km from the storm. A 10-cm spherical electric antenna is located 2 m above the ground and two perpendicular magnetic loop antennas have an effective surface area of 2×48 m^2. The vertical upward electric field component and horizontal eastward and southward magnetic field components (geographic orientation) are sampled at 50 kHz. Every 5 min 144 s long waveforms are recorded, followed by 156 s of idle time (Santolík & Kolmašová, 2017).

A two-component VLF receiving station of the Sodankylä Geophysical Observatory of the University of Oulu is placed at a remote, low noise site in Kannuslehto, Finland (67.7°N, 26.3°E) at a distance of ∼2,100 km from the thunderstorm. VLF electromagnetic waves are recorded in a frequency band from 0.2 to 39 kHz by two orthogonal magnetic loop antennas oriented in the geographic north-south and west-east directions. Each antenna has an effective surface area of 1,000 m^2. The sampling frequency is 78.125 kHz (Manninen et al., 2016).

A sudden ionospheric disturbances (SID) monitor of the Slovak Organization for Space Activities placed in Bojnice, Slovakia (48.8°N, 18.6°E) is used for the monitoring of perturbations of narrow band VLF signals emitted by strong transmitters for communication with submarines in a frequency range from 15 to 30 kHz. The SID monitor is able to monitor simultaneously the strength of up to 16 VLF transmitter signals. The sampling frequency is 1 Hz. For this study we have chosen the recordings of the carrier of the VLF transmitter DHO38 used by the German Navy. The transmitter is located near Rhauderfehn, Germany (53.1°N, 7.6°E). DHO38 transmits at a frequency of 23.4 kHz with a power up to 800 kW. The transmitted signal propagates from Germany to the receiver in Slovakia via multiple reflections between the Earth and the lower ionosphere. The shortest distance between the signal propagation path and the thunderstorm location was ∼300 km.

The Hylaty ELF receiving station is located in an uninhabited area in the Bieszczady Mountains (49.2°N, 22.5°E) in Poland at a distance of 730 km from the thunderstorm. It is operated by the Jagiellonian University and the AGH University, Krakow. Two magnetic field components oriented in the geographic north-south and east-west directions are sampled at a frequency of 887 Hz. The frequency bandwidth of the receiver extends from 0.03 to 300 Hz (Kulak et al., 2014). Current moment waveforms and charge moment change waveforms are reconstructed from the ELF measurements of magnetic field fluctuations using the inverse channel method (Kulak & Mlynarczyk, 2013).

Monitors of quasistatic vertical electric field changes (BTD-300) have been designed, constructed and operated by Biral, a UK manufacturer of meteorological and visibility sensors (Bennett, 2013, 2017). The frequency of the BTD-300 ranges from 1 to 45 Hz. The sensors detect the signal induced on three co-located metallic electrodes when exposed to changes in surrounding atmospheric electric field produced by lightning discharges. Each electrode generates a displacement current, flowing from the surface of the conductor to the ground, which corresponds to the rate of change of the local electric field, measured with an electrometer current amplifier and sampled at 100 Hz. The detector uses passive electrodes of approximately 0.1 m^2 each, whose geometry has been chosen to inhibit corona initiation in local thunderstorm strong electric fields. For this particular geometry of the detector and antennas, only lightning discharges produce the correct combination of relative signal amplitudes at different antennas compared to local sources of displacement currents that are not associated with lightning. To help differentiate lightning-related signal, the covariance plots between the primary and secondary antennas are used. As the detectors were able to record signals associated with distant sprites (Füllekrug et al., 2013) and halos (Bennet, 2014) due to extensive horizontal changes in the low ionosphere electron density, we expected them to detect also signals related to elves. In order to discriminate signals associated with elves from signals generated by close lightning, we have used the data recorded at two stations, Chilbolton (51.2°N, 1.4°W) and Portishead (51.5°N, 2.8°W) in the UK located at a distance of 1,040 and 1,140 km from the storm, respectively.

To get an overview of the lightning activity during the investigated thunderstorm, we used a list of lightning detections provided by the European Cooperation for Lightning Detection (EUCLID). EUCLID network consists of more than 150 sensors in 27 countries and covers whole Europe ranging from Portugal to Finland and from Sicily to the North of Norway. The detection efficiency for Austria (closest country to Czechia) is 98% and 84% for negative flashes and strokes, respectively; and 97% and 92% for positive flashes and strokes, respectively. The mean location accuracy is 500 m (Schultz et al., 2016). EUCLID reports the time of lightning occurrence with microsecond precision, the location, the type (IC/CG) of the discharge, its peak current and the polarity for each identified stroke. The estimation of the peak current is based on the transmission line model and on the conversion of peak field to peak current assuming a return stroke speed of 1.2×10^8 m/s. Estimated typical errors of the peak current for positive strokes is 4% and might reach up to 40% (Poelman et al., 2016; Schultz et al., 2016). The automated detection procedures developed for operational service delivery have on occasion difficulties with the locations of extremely strong lightning strokes because of complexity of their field waveforms. This might happen when numerous sensors saturate, strong ionospheric reflections occur or when the actual return stroke to ground is preceded by numerous recoil leaders producing return stroke type field pulses (Cummins, 2000).

Locations of all positive (red points) and negative (blue points) CG lightning discharges detected by EUCLID in the latitude/longitude range [49.0°N-50.5°N] and [12.0°E-14.0°E] during the evolution of the thunderstorm are shown in Figure 2.

4. Measurements

4.1. Optical TLE Detections

Our data set is built around the first optical observations of elves above Czechia. Four clearly visible elves were captured in four different 40 ms long video frames at the observational site in Nydek, Czechia on April 2, 2017: the E1 frame starting at 19:21:36.185 UTC, the E2 frame starting at 19:39:23.901 UTC, the E3 frame starting at 19:53:14.028 UTC, and the E4 frame starting at 20:05:12.835 UTC. For the first three frames (E1, E2, and E3) we have GPS timing with an accuracy better than 1 ms but the last frame E4 was recorded only by a camera without the GPS time tag, using an approximate computer time with an accuracy of 100 ms. The elves E1, E2 and E3 were also captured by this camera, and we show its relevant video frames from the four elves in Figure 3. The altitudes of the centers of elves are estimated ∼80–86 km using the elevation above horizon and the known distance to the storm. These heights are by several kilometers lower than those of van der Velde and Montanyà (2016) in the Mediterranean region. As the edges of elves are usually quite diffuse, we estimated their lateral extent and the hole radius only very roughly. We visually determined the azimuths of the centers, inner and outer edges of the four captured elves. Knowing the location of causative RS and thus their distance to the camera, we calculated the inner and outer radii of individual elves. To make the estimation of the elves radii more reliable, we repeated their visual rough estimation a few times within a month. We calculated average values of these estimates, which are illustrated in Figure 3 by blue dots. The fluctuations in our visual estimates are represented by inaccuracies of elves radii. The inner radius varies from 29 to 48 km (E1: 41 ± 2 km; E2:45 ± 3 km; E3:33 ± 2 km; E4:29 ± 3 km) the outer radius reaches 112–183 km (E1: 175 ± 7 km; E2:143 ± 2 km; E3:148 ± 4 km; E4:114 ± 2 km). Additionally, we also very roughly estimated brightness of elves by comparing them with the brightness of stars in the field. We constructed reference frames by averaging several video frames neighboring the elves to minimize the noise. We subtracted these reference frames from the corresponding frames, which contained the elves. As a result, we obtained the brightness of the elves themselves. We then measured the brightness of stars in the reference frames in order to obtain a relation of the brightness in our video and catalog magnitudes of the stars. The total apparent magnitude of the elves E1 was approximately −7. The relative brightness of elves E2, E3, and E4 with respect to E1 reached 80%, 80%, and 50%, respectively. All optical properties of elves are summarized in Table 1. Additionally, two sprites were observed during the same thunderstorm. The frame containing the first sprite started at 19:26:37.284 UTC. The second sprite was captured shortly after the elves E3 by the camera without the GPS timing, in the frame starting 19:53:14.121, tagged only with an accuracy of 100 ms. The thunderstorm persisted for ∼7 h. We focus on its electrically most active part, which started approximately 1 h after sunset at 18:30 UTC and continued until 22:30 UTC. The cameras were operational from the sunset until the sunrise on the next day.

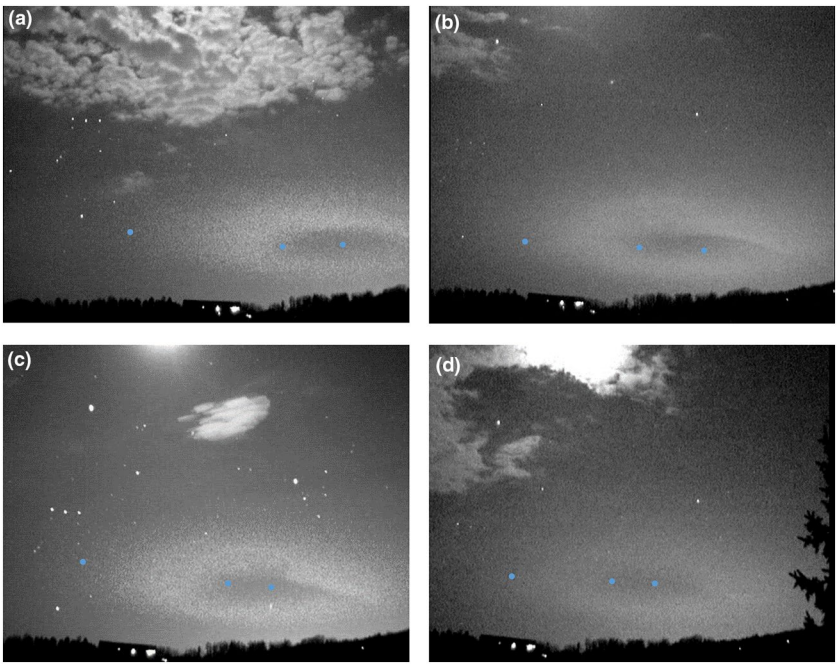

Figure 3. Pictures of elves captured on April 2, 2017 by the Watec 910HX camera in Nýdek (Czechia) at a distance of 430 km from the thunderstorm (a) E1: 19:21:36.185–19:21:36.225 UT; (b) E2: 19:39:23.901–19:39:23.941 UT; (c) E3: 19:53:14.028–19:53:14.068 UT; (d) E4: within 100 ms around 20:05:12.8 UT. Blue dots represent very rough visual estimates of the centers, inner and outer edges of elves.

4.2. Measurements of the EUCLID

During the time interval from 18:30 to 22:30 UTC, 142 CG and 656 IC lightning discharges were detected by EUCLID in the corresponding area restricted by the latitudes from 49.0°N to 50.5°N and longitudes from 12.0°E to 14.0°E. The fraction of positive CG lightning strokes which occurred during the investigated thunderstorm reached 55%. This was unusually high compared to the average fraction of positive strokes occurring in Europe during April, which is about 19% as reported by EUCLID (Poelman et al., 2016) while this fraction reaches about 20% from December to February and around 10% from June to October. The average annual fraction of positive lightning detected in Czechia in the period 2002–2008 was also 19% (Novak & Kyznarova, 2011). The observed fraction of 55% is also much higher than the largest reported average fractions of positive strokes observed at different continents during the winter season (Japan—33%, Wu et al., 2014; Central United States—20%, Market & Becker, 2009; Eastern Mediterranean—13%, Ben Ami et al., 2015). Thus, we cannot exclude that the analyzed storm had an inverted-polarity electrical charge structure, which is predominantly observed for dry continental regions and in which fractions of CG+ lightning strokes might exceed 80% (MacGorman et al., 2005). The positive CG lightning discharges were also exceptionally strong reaching nearly 500 kA. The peak current of negative and positive CG lightning strokes ranges from −2 to −42 kA and 9 to 493 kA, respectively. Median peak currents for positive and negative CG strokes that occurred during the thunderstorm were +64 kA and −5 kA, respectively. The mean peak currents were +93 kA and −9 kA. An abnormality in strengths of the positive peak currents is also supported by findings of Novak and Kyznarova (2011) who reported that the distribution of peak currents of positive lightning in Czechia is peaking at +4 kA and that there were less than 1% of currents above +50 kA in the period 2002–2008. The observed large median positive peak current of 64 kA is probably even underestimated because of the difficulties of the EUCLID network to identify some of the extremely large peak current discharges. The temporal distribution of negative (blue stars) and positive (red stars) peak currents is shown in Figure 4a. The green dashed vertical lines indicate the occurrence of elves. The horizontal red dashed line in Figure 4a represents a peak current of 100 kA, which we choose as a reference for strong strokes as estimated by EUCLID. There are 23 positive strokes with peak currents above this 100 kA threshold. Taking into account an uncertainty of the EUCLID current estimation (absolute peak current deviations of about

Journal of Geophysical Research: Atmospheres

10.1029/2020JD032825

Table 1
Properties of Four Elves, Two Optically Not Detected Elves, Properties of Their Causative Strokes, Properties of Other 8 Strong Strokes

	Hole radius (km)	Outer radius (km)	Brightness relative to event E1 (%)	Peak current (kA) EUCLID	Peak current (kA) from VLF Rustrel	Peak current (kA) from VLF KAN	Current moment (kA.km)	CM FWHM (ms)	Charge moment change (C.km)	Photometer peak value (a.u.) Přimda	Photometer peak value (a.u.) Kocelovice	Photometer FWHM (ms)	Covariance (V^2) from Chibolton	Covariance (V^2) from Portishead
E1	41 ± 2	175 ± 7	100	X	X	433	160	1.2	400	79,316	99,684*	1.2	16,934	1,932
E2	45 ± 3	143 ± 2	80	493	(298)	439	95	2.3	350	442,284	96,326*	0.4	33,817	3,978
E3	33 ± 2	148 ± 4	80	X	X	419	120	2.6	600	282,224	225,814*	0.3	18,221	1,850
E4	29 ± 3	114 ± 2	60	391	(278)	404	75	2.3	200	1,552,544	56,103*	0.5	4,441	892
E5?	X	X	X	X	307	361	90	1.7	200	56,749	3,618,186	0.6	2,222	404
E6?	X	X	X	363	X	441	80	1.6	222	159,997*	11,862*	X	2,171	282
S2				248	242	266	320	1.3	610	540,576	13,190	0.7	<1	<1
S4				98	79	85	65	2.2	150	2,690,528	2,419*	0.4	<1	<1
S5				188	230	183	250	1.6	450	1,332,768	13,020	1.5	<1	<1
S6				106	129	116	80	1.6	400	998,944	3,634	1.3	<1	<1
S7				129	129	95	95	1.6	600	1,616,864	3,041*	0.5	3	2
S12				119	100	79	38	1.6	60	2,150,392	2,888	1.0	2	<1
S14				251	251	203	240	1.3	400	58,491	4,007,424	0.9	<1	6
S20				242	218	279	75	2.4	200	144,963*	9,377*	X	<1	1

Note. The two values in brackets in the column 6 (Peak current derived from VLF Rustrel) are underestimated because of preamplifier saturation effects on the VLF magnetic loop antenna in Rustrel. The values marked by a star in columns 11 and 12 (Photometer peak values) indicate measurements at a low sampling rate of 500 Hz.

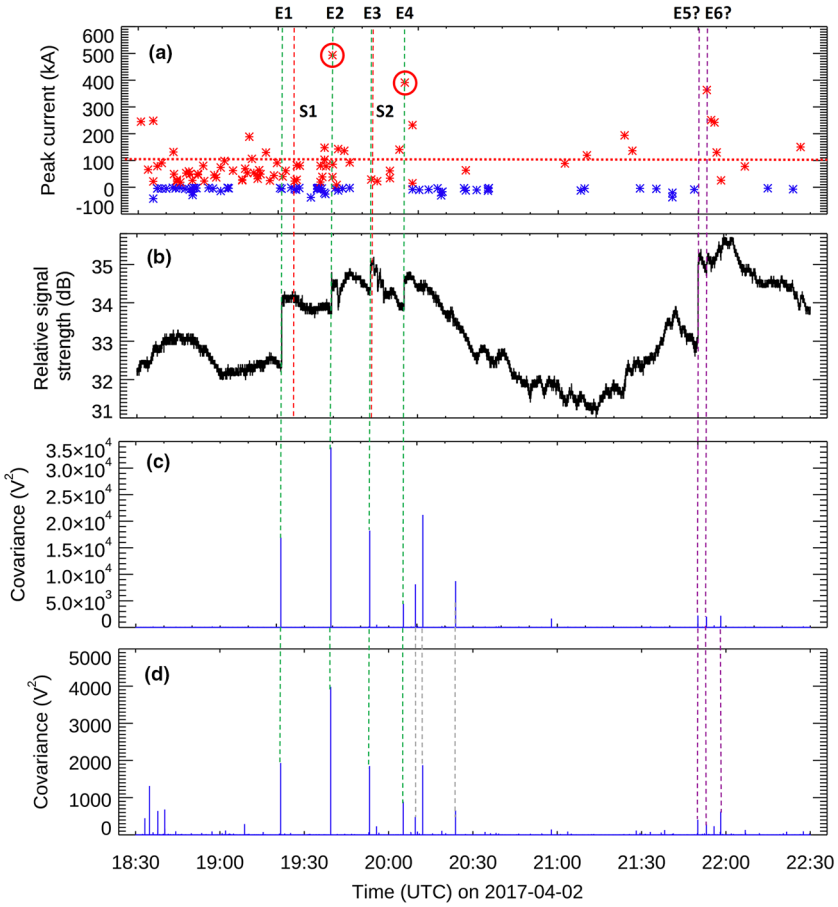

Figure 4. (a) The time distribution of negative (blue stars) and positive (reds stars) peak currents. The green dashed vertical lines indicate the times of elve occurrences. The peak currents of causative strokes of elves E2 and E4 are highlighted by red circles. The horizontal dashed line represents a peak current value of 100 kA. (b) The intensity of the DHO38 transmitter signal recorded in Bojnice (Slovakia). (c and d) Covariance plots calculated from the measurements of displacement currents conducted in Chilbolton (c) and Portishead (d), corresponding to the rate of change of the local electric field. Vertical gray dashed lines point to strong strokes that accompanied an unrelated storm located in Switzerland. Purple dashed lines are associated with strokes that might produce undetected elves. Red vertical dashed lines in panels (a and b) indicate the occurrence times of sprites S1 and S2.

4 kA in comparison with direct current measurements; Schulz et al, 2014), we included in our data set also one stroke with a peak current of 98 kA. We attempted to identify locations and times of occurrence of the source lightning strokes of four observed elves in the EUCLID data. However, for only two of them, we found reliable unambiguous detections. (Note: we identified all source lightning strokes in the VLF and ELF data). Frame E2 corresponds to a positive CG stroke detected at 19:39:23.926 UTC with a peak current of +493 kA and with a reasonable agreement of a high number of EUCLID sensors on this large signal peak. Frame E4 corresponds to a positive CG stroke at 20:05:12.835 UTC and with a peak current of +391 kA for which a number of sensors reported consistent high amplitude data. The correspondence is again unambiguous, as no other lightning discharges have been detected in the analyzed area during the 2 min before and after this event. These two estimates of the peak currents of causative strokes for elves are marked by red circles in Figure 4a.

As a result, the EUCLID estimates of the peak currents for the other two causative strokes are uncertain. During the video frame E1, a complex positive discharge has been detected at 19:21:36.195 UTC, probably with a large number of recoil leaders where the EUCLID sensors did send numerous messages, causing difficulties to select the sensor reports correlated with the main return stroke. For frame E3, EUCLID sensors sent many messages around 19:53:14.612 UTC and no consistent detection of a lightning stroke was possible, probably because of its very large electromagnetic pulse that led to strong ionospheric reflections.

4.3. Subionospheric VLF Propagation and Additional EUCLID Measurements

The intensity of the DHO38 transmitter signal exhibits several steep increases (Figure 4b) at the times of the optical detections of elves. The increases of the intensity of a VLF signal can be recognized as LOREs (Haldoupis et al., 2013) and explained by a smaller attenuation of a propagating signal at the reflection point above the thunderstorm region due to an increased ionization of the lower ionosphere caused by elves. Besides the four increases of the signal strength which coincide in time with the optical observations of elves we noted two additional rapid intensity increases (one very large and one very weak) at 21:50 and 21:53 UTC, respectively. We speculate that optically undetected elves ("E5" and "E6") might also have occurred at the times of these signal intensity increases. These elves might have been out of the field of view of the camera or might have been too faint to be detected by the UFOcapture software.

This is confirmed by EUCLID measurements. For event E5 the sensor data show a large electromagnetic peak at 21:50:00.417 UTC, when six close sensors were saturated. The peak current reported by other sensors at the same time were inconsistent, probably as a result of strong ionospheric reflections. The second of these hypothetical elves (event E6) was associated with a strong positive return stroke having a peak current of +363 kA in the EUCLID database.

4.4. QuasiStatic Current Changes

Figures 4c and 4d represent 4-h long covariance plots calculated from the measurements of quasistatic displacement currents conducted on the BTD-300 detectors at Chilbolton (Figure 4c) and Portishead (Figure 4d). The prominent peaks in the covariance plots detected simultaneously at both stations indicate the presence of distant ionospheric electron density enhancements, resulting from intense lightning electromagnetic pulses. The green dashed vertical lines show that the peaks in the covariance plots exactly correspond to the times of the elve observations. There are also detections of other covariance peaks by both the Chilbolton and Portishead monitors. Three pairs of peaks interconnected by vertical gray dashed lines belong to strong strokes which are associated with a nonrelated storm located in Switzerland (~9.3°E; ~47.3°N) and which probably also modified the ionospheric conductivity. Three weaker pairs of peaks indicated by purple dashed lines are associated with strokes, which occurred during the investigated time interval close to the thunderstorm in Czechia. The first event at 21:50 UTC coincides with the event E5 where a substantial increase of the strength of the VLF transmitter signal was detected, as it is shown in Figure 4b. The second pair of peaks corresponds to a weak increase of the VLF signal at 21:53 UTC, with the EUCLID detection of a +363 kA CG stroke, marked as event E6. For the third one at 21:58 UTC no distinct VLF signal increase was observed, suggesting the associated strokes originated from a different area far from the VLF transmission path.

Surprisingly, no pairs of peaks in covariance plots were associated with other strong strokes with peak currents exceeding 100 kA. This indicates that these strong strokes did not generate an extensive horizontal ionospheric electron density enhancement related to elves.

4.5. VLF Measurements of Causative RS

As the next step, we tried to independently verify the values of peak currents using the three-component VLF measurement in Rustrel, France and the two-component VLF measurement in Kannuslehto, Finland. As the thunderstorm was well localized and far from both receiving sites, the distance and angle or arrival was very similar (<3% difference) for ground wave magnetic field pulses emitted by all investigated RS. As the magnetic loop antennas are directional with cosine characteristics, we corrected the observed magnetic field peak amplitudes for their angle of arrivals. We assume that after the correction the observed magnetic field peak amplitudes were proportional to their source peak currents (Uman et al., 1975).

Due to our VLF recording pattern in Rustrel (a cycle of 144 s recordings followed by 156 s dead time) we recorded only two RS pulses associated with elves from frames E2 and E4, one RS pulse associated with an optically nondetected event E5 and some other eight return stroke pulses from lightning discharges with peak currents exceeding 100 kA. Using the same method as Santolík and Kolmašová (2017), we verified

the angle of arrival of the observed RS pulses to confirm that these pulses traveled to the VLF receiver from the azimuth of the investigated thunderstorm. With minor corrections of amplitudes of the magnetic field ground waves for their angles of arrival, E-W magnetic field waveform snapshots for all analyzed strong RS pulses are shown in Figure 5a. Waveforms belonging to strokes that produced the elve events E2 and E4 are represented by red solid lines. The waveform shown by a red dotted line belongs to the stroke corresponding to the optically nondetected event E5. Waveforms generated by other strong strokes with peak currents above 100 kA are plotted in black. All signals generated by RSs associated or possibly associated with elves are followed by unusually strong ionospheric reflections of higher order that sometimes reach the analog saturation level of our distant receiver. Ionospheric reflections, also known as sky waves, are labeled in Figure 5a as SW1, SW2, SW3,..., according to their order; the saturation is also indicated. We calculated the amplitudes of the E-W RS ground wave peaks and plotted them in Figure 5b as a function of the known peak currents provided by EUCLID. Strokes associated with events E2, E4, and E6 are represented by red dots; other strong strokes are shown by black dots. In other words, each black line from panel a is represented by a black filled circle in panel b, which shows the peak amplitudes of the ground waves of RSs as a function of known peak currents. We displayed in green also peak amplitudes belonging to nine +CGs stronger than 30 kA occurring during the storm.

The blue dashed line in Figure 5b represents a linear relation (Uman et al., 1975) calculated using a least squares regression. For calculation of the coefficient of a linear relation, we used all positive strokes above 30 kA for which were both VLF amplitude of the E-W RS ground wave and peak current known. The drop of E2 and E4 peak amplitudes can be explained by analog saturation effects in the preamplifier, which are well seen on the subsequent sky waves. Therefore, we omitted these two points and calculated the coefficient of the linear relation only for peak amplitudes of ground waves with amplitudes below the saturation level of approximately 28 nT. The red circle marked E5 shows a peak current estimate (+307 kA) for a known magnetic field peak amplitude of the corresponding ground wave RS pulse, while the red circle marked E6 represents a magnetic field peak amplitude estimate for a known peak current (+363 kA) associated with the detected RS. The VLF amplitudes of the RS ground waves, as well as the coefficient of linear relation calculated using the N-S magnetic field component differed only by 4.6% on average from the values received from the E-W magnetic field measurements.

As the receiving station Kannuslehto operated continuously, we were able to find RS signals belonging to events E1–E6 in the recordings of horizontal magnetic field components. We used records of the southward magnetic field component for an estimation of the peak amplitudes of the RS ground wave pulses, as their values in the eastward component reached the saturation level of the receiver. Similarly, as in Rustrel, the ionospherically reflected waves of higher order associated with elves events were unusually strong, saturating the receivers of both magnetic field components. We have also estimated the peak amplitudes of RS ground wave pulses for a set of 10 strong RSs (above 100 kA; eight of them detected in Rustrel). We corrected the amplitudes of the magnetic field ground wave pulses for their angles of arrival and plotted them in Figure 5c as a function of the known peak current provided by EUCLID. Strokes associated with events E2, E4, and E6 are represented by red dots, other strong strokes are shown by black dots. The blue dashed line in Figure 5c again represents a linear relation calculated using a least squares regression. The red circles marked E1, E3, and E5 shows a peak current estimate (+433 kA, +419 kA, and +361 kA) for known magnetic field peak amplitudes of the corresponding ground wave RS pulses. With these estimates, peak currents of all lightning RS causing the observed or anticipated elves events E1–E6 are above 300 kA. Measured peak values of recorded RS pulses and peak currents inferred from the VLF measurements are shown in the Table 1.

4.6. Optical and ELF Measurements of RS

In order to find an explanation for the observed absence of elves for RS with peak currents between 100 kA and 300 kA we have also inspected other independent measurements of RS manifestations—light curves measured by fast photometers, as well as current moments and charge moment changes reconstructed from the ELF magnetic field measurement.

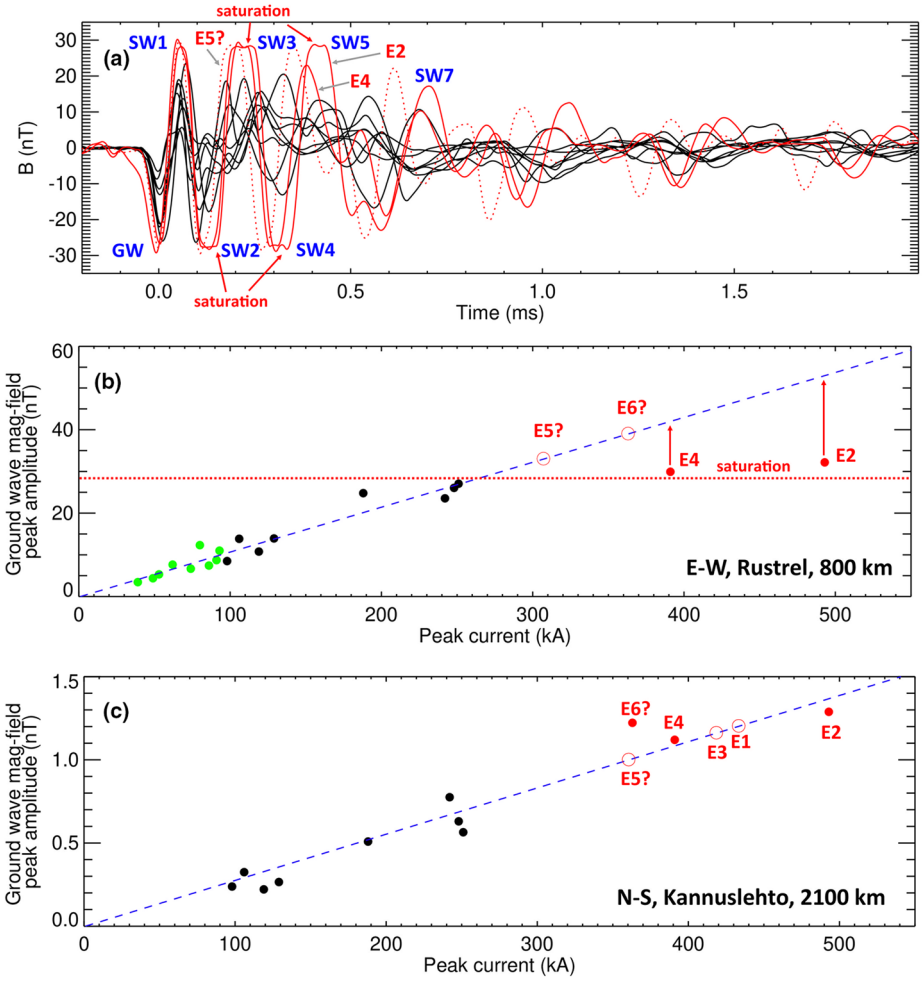

Figure 5. (a) E-W magnetic field waveform snapshots recorded in Rustrel, France (each of them 2.2 ms long, starting 200 μs prior to their ground wave peaks). The waveforms that belong to elves produce the strokes E2 and E4 are represented by red solid lines, the waveform belonging to possible elves-producing stroke E5 is shown by a red dotted line. All waveforms generated by other strong strokes are plotted in black. Ground and sky waves are labeled by GW and SW. (b) Ground wave peak amplitudes of all positive return strokes (RS, $I_p > 30$ kA) as a function of the peak currents provided by EUCLID (green and black dots correspond to peak currents below and above 100 kA, respectively). The blue dashed line represents a linear regression line without elves producing strokes where preamplifier saturation at approximately 28 nT occurred (marked by a red dotted line). The red open circle marked "E5?" shows a current estimate for a known magnetic field peak amplitude. The red open circle "E6?" shows a magnetic field amplitude estimate for a known peak current. (c) The same as in panel (b) but for the measurements conducted in Kannuslehto, Finland. The red open circles marked E1, E3, and E6 show current estimates for known magnetic field peak amplitudes. Red bullets show the strokes for which both the peak currents and VLF waveforms were available.

Fast all-sky photometers located at a distance from 20 to 100 km from the observed lightning channels captured light curves for all four elve-producing RSs, two optically nondetected elve-producing RSs and also the 20 other strong RS with peak currents above 100 kA which occurred during the observed thunderstorm. Note, that all-sky photometers captured also the scattered light from the clouds. Examples of the obtained RS light curves are shown in Figures 6a and 6c for elves-parent events E2 and E4 and in Figures 6b and 6d for strong strokes with peak currents of +232 kA and +248 kA, which, however, did not generate any observable elves signatures. The subsequent pulses occurring in Figures 6c and 6d probably belong to subsequent RS. The light curve in Figure 6d corresponds to a stroke detected by EUCLID with a surprisingly small peak current of +15 kA. We did not found a relevant EUCLID detection in the time of the second peak in Figure 6c. The distances between the observed RS and the corresponding photometers were 100, 23, 31, and 25 km, respectively, for the events shown in Figures 6a–6d. The light curves for elves E1–E5

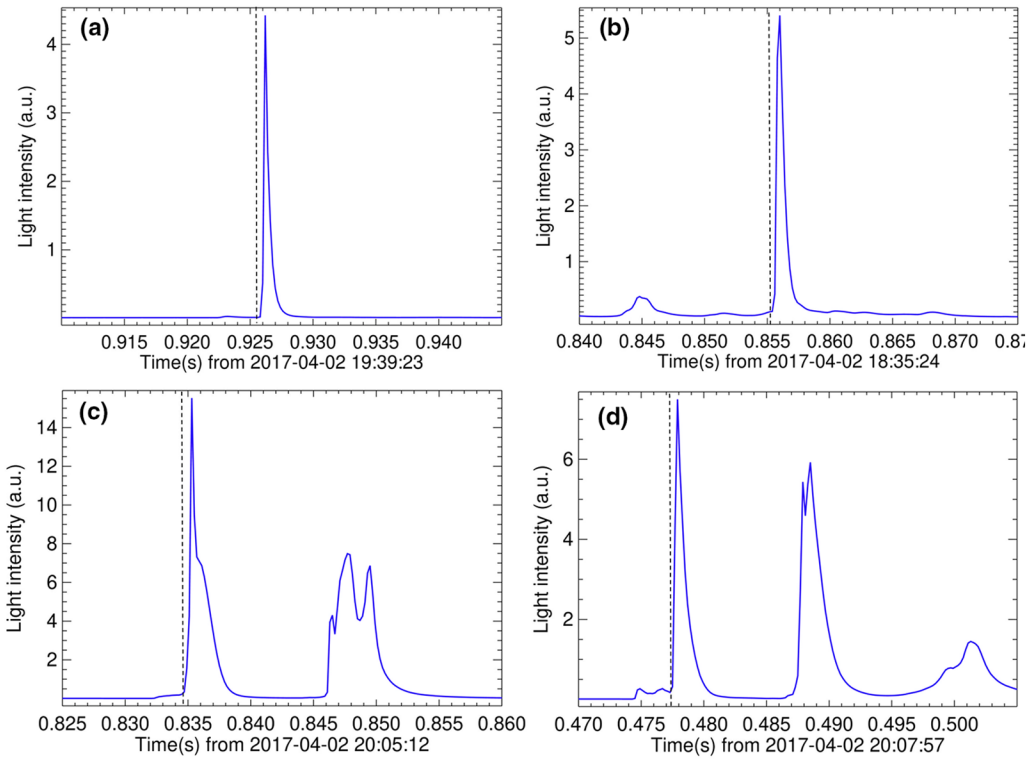

Figure 6. Examples of light curves of return stroke discharges measured by high-speed photometers of the Czech fireball network at distances D from the RS channel. (a) E2: D = 100 km; (b) RS with a peak current of 248 kA, D = 25 km; (c) E4, D = 31 km; (d) RS with a peak current of 231 kA, D = 23 km. Vertical dashed lines show the time of occurrence of RSs as reported by EUCLID.

and for 15 strong strokes were recorded with a sampling frequency of 5 kHz; the light curves of elves E6 and four remaining strong strokes were sampled only at 500 Hz. The measurement was not fast enough to derive the velocity of the RS current waveform the rising times from their light curves. We are also not able to relate their peak amplitudes and peak currents as changes in the visibility between locations of lightning discharges and receiving station (for example, due to heavy precipitation) might have influenced the amplitudes of light curves. Therefore, we characterize the light curves of individual lightning by full width at half maximum (FWHM) of the RS luminosity pulses. We used only records sampled at 5 kHz. The FWHM is 0.6 ± 0.3 ms and 0.8 ± 0.3 ms for elves producing and the other strong strokes, respectively. As the spread of FWHM values is quite large, we concluded that there is no apparent difference between light curves of elves producing strokes and the light curves of other strong strokes (Table 1).

Similarly, current moment curves do not show any apparent differences between those calculated from the ELF magnetic field measurement for elve-producing RS and other strong RS that occurred during the same thunderstorm. Examples of current moment curves belonging to the same RS as in Figures 6a–6d are plotted in Figures 7a–7d. We calculated average current moment and charge moment changes separately for elve-producing strokes and for the other strong strokes. The obtained average peak current moments and its standard deviations are 103 ± 29 kA.km for strokes with observed elves signatures, and 125 ± 85 kA. km for other strong strokes with peak currents above 100 kA that occurred during the observed thunderstorm. The corresponding average charge moment and its standard deviations changes are 301 ± 155 and 329 ± 143 C.km, respectively. We did not find any relation between peak currents and charge moment change values for elves producing strokes (Table 1) which is in agreement with Huang et al. (1999). Taking into account a huge spread of values we conclude that these average numbers do not differ significantly for both groups of strokes. We also obtained similar values of FWHM for current moment pulses: 2.1 ± 0.3 ms and 1.8 ± 0.3 ms for elves producing and the other strong strokes, respectively. Unfortunately, in both groups of strokes, several current moment curves exhibited signatures of continuing current, which caused the broadening of pulses and made the comparison of shapes of current moment pulses unusable.

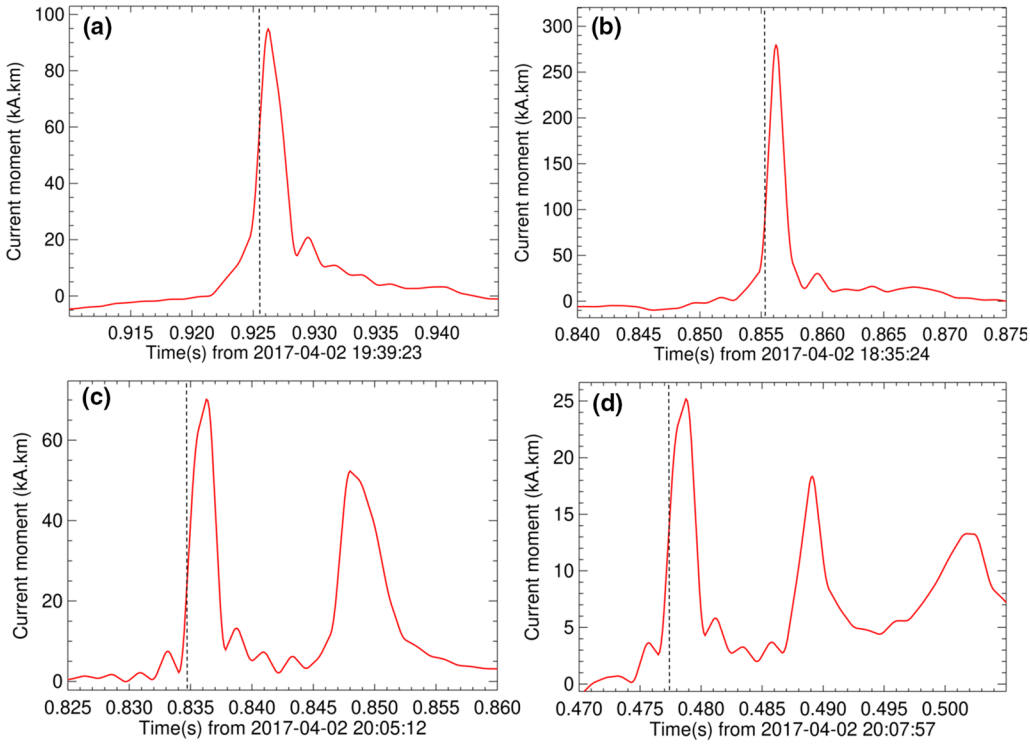

Figure 7. Examples of current moment curves of elve-producing RS (a and c) and other strong RS (b and d) calculated from the ELF magnetic field measurements conducted at Hylaty station (Poland) at a distance of about 730 km from the thunderstorm. The same events as in Figure 6 are shown. Vertical dashed lines show the time of occurrence of RSs as reported by EUCLID. The propagation delay was already taken into account.

5. Model of Elves

We have shown that measurements of the current moment curves, charge moment changes, and the shapes of light curves of individual RS do not provide us with the possibility to predict if individual strokes produced elves or not. On the contrary, measurements of displacement currents and electromagnetic VLF signals indicate extensive ionospheric disturbances as manifestations of RSs associated with elves, even without their optical records. However, using any of the described measurements we are not able to explain why only lightning strokes with extremely high peak currents above 300 kA (and larger time derivative of the electric field they generated) were associated with elves in our observations, and why the published lower limits (Blaes et al., 2016; Newsome & Inan, 2010; van der Velde & Montanyà, 2016) give a broad range of very different values.

It is evident that there is another return stroke property, which is controlling the elves generation. We therefore simulated optical emissions in the lower ionosphere associated with RS peak currents as high as 100 and 300 kA in order to identify other RS parameters which were not covered by our measurements and which might influence the inception of elves.

To simulate the RS process, we use a modified transmission line model with an exponential current decay with height (MTLE) which is an "engineering" RS model (Rakov & Uman, 1998). For this model the current pulse at a given height z is related to the current pulse at the bottom of the channel by the formula:

$$I(z,t) = I(0,t - z / v)\exp(-z / \lambda), \quad (1)$$

where λ is the attenuation length scale that we used to simulate a conductivity of the return stroke lightning channel and v is the RS current front wave velocity. The exponential decay of the current amplitude with the altitude in our model is in accordance with Zhang et al. (2019) who showed that an exponential approxima-

tion of the attenuated current front is reasonable for strong discharges. Their measurements show generally lower values of the attenuation length scale (76–724 m), but we have tentatively chosen also higher values of this variable (300, 500, 1,000, and 1,500 m) to show the impact of the conductivity of the RS channel on the intensity of the elves. The attenuation length and the current wave velocity are independent in our model. $I(0,t)$ is a base current at $z = 0$ characterized by the analytical formula in Equation 22 from Heidler and Cvetić (2002) with typical parameters for the first RS from Table 1 in Heidler and Cvetić (2002). A development of the channel base current with a maximum value of 100 and 300 kA is shown in Figures 8a and 8b, respectively. For the elves simulations we first computed an electromagnetic field in a vacuum produced by the RS in the same way as Marshall et al., (2010). The interaction of the electromagnetic wave with the lower ionosphere is similar to the model of Veronis et al., (1999). We solve Maxwell's equations self-consistently; taking into account ionization, electron attachment, and effects of electron mobility on the conductivity of the discharge channel. Excitation of the first positive band of nitrogen is derived from kinetic models (Veronis et al., 1999) who determined an excitation threshold of the first positive band of nitrogen as one third of the characteristic breakdown field E_k. The neutral density profile was taken from the MSIS-E-90 Atmosphere Model (Hedin, 1991). The ambient electron density was modeled by a double exponential function after Kuo et al. (2007)

$$N_e(t = 0) = 1.43 \cdot 10^7 \exp(-0.15h)\exp\left[(\beta - 0.15)(z - h)\right], \quad (2)$$

with an ionospheric sharpness parameter $\beta = 0.5\text{km}^{-1}$. The height of the bottom of the ionosphere $h = 86$ km was derived from our optical observations using the method described in van der Velde & Montanyà, 2016. A length of the lightning channel is chosen equal to 7.5 km according to a hypothetical position of the main positive charge center derived from meteorological radar measurements of the cloud-top height and from balloon measurements of Stolzenburg and Marshall (2008). Nevertheless, we admit that charge distribution in different storms may alter substantially (especially in possible case of an inverted polarity charge structure) and therefore we run the simulations also for lower altitudes of the main positive charge centers. Figure 8 illustrate the power density of emitted light expressed as production rate of photons per cubic meter per second for different RS current wavefront velocities (20%, 40%, and 60% of the speed of light), a constant attenuation length $\lambda = 500\,\text{m}$, and two peak currents (100 kA panels on the left; 300 kA panels on the right). Our choice of current wave velocities is based on findings of Mach and Rust (1993) and Blaes et al. (2014). Mach and Rust reported current wave velocities as low as 17%–40% of the speed of light for positive lightning. Blaes et al. (2014) found that the most probable speed estimate was 64% of the speed of light for elves producing lightning. The number of photons per cubic meter per second for different attenuation lengths λ (300, 500, 1,000, and 1,500 m), a fixed RS current wave velocity equal to one third of the speed of light, and two peak currents is illustrated in Figure 9 (100 kA panels on the left; 300 kA panels on the right).

It is obvious from Figures 8 and 9 that both a slower current wavefront and a higher resistivity of the lightning channel represented by a decreasing attenuation length λ lead to a weaker emission of photons. If we decrease the parameter λ to one fifth from 1,500 to 300 m, the emission of photons decreases by two orders of magnitude. Similarly, if we decrease the velocity of the RS current wave 3 times from 60% to 20% of the speed of light, the emission of photons drops by two orders of magnitude. The maximum value of 2.1×10^{13} photons/s/m^3 we obtained for a peak current of 300 kA, a velocity of the current wave of 1.8×10^8 m/s and an attenuation length of 1,500 m (Figure 9h). The photon production was one order of magnitude smaller if we keep all parameters and decrease the peak current of the causative stroke to 100 kA. To be sure that our model gives us reasonable values of the photon production, we very roughly approximated a photon flux which might see a sensor onboard the FORMOSAT-2 spacecraft (A. B. Chen et al., 2008, their Figure 5) generated by the simulated elve from Figure 8c. We obtained a flux of about 10^3 photons/cm^2 corresponding to a peak current of 110 kA in their Figure 5, which is in a good agreement with our model. A threshold for the electric field at elves altitude needed for their generation (0.3 E_k, Veronis et al., 1999) was reached for all simulated combinations of parameters. For the least favorable conditions represented by a peak current of 100 kA, the current wave velocity of one third of c and an attenuation length of 300 m we obtained an electric field of 0.37 E_k at an altitude of 89 km.

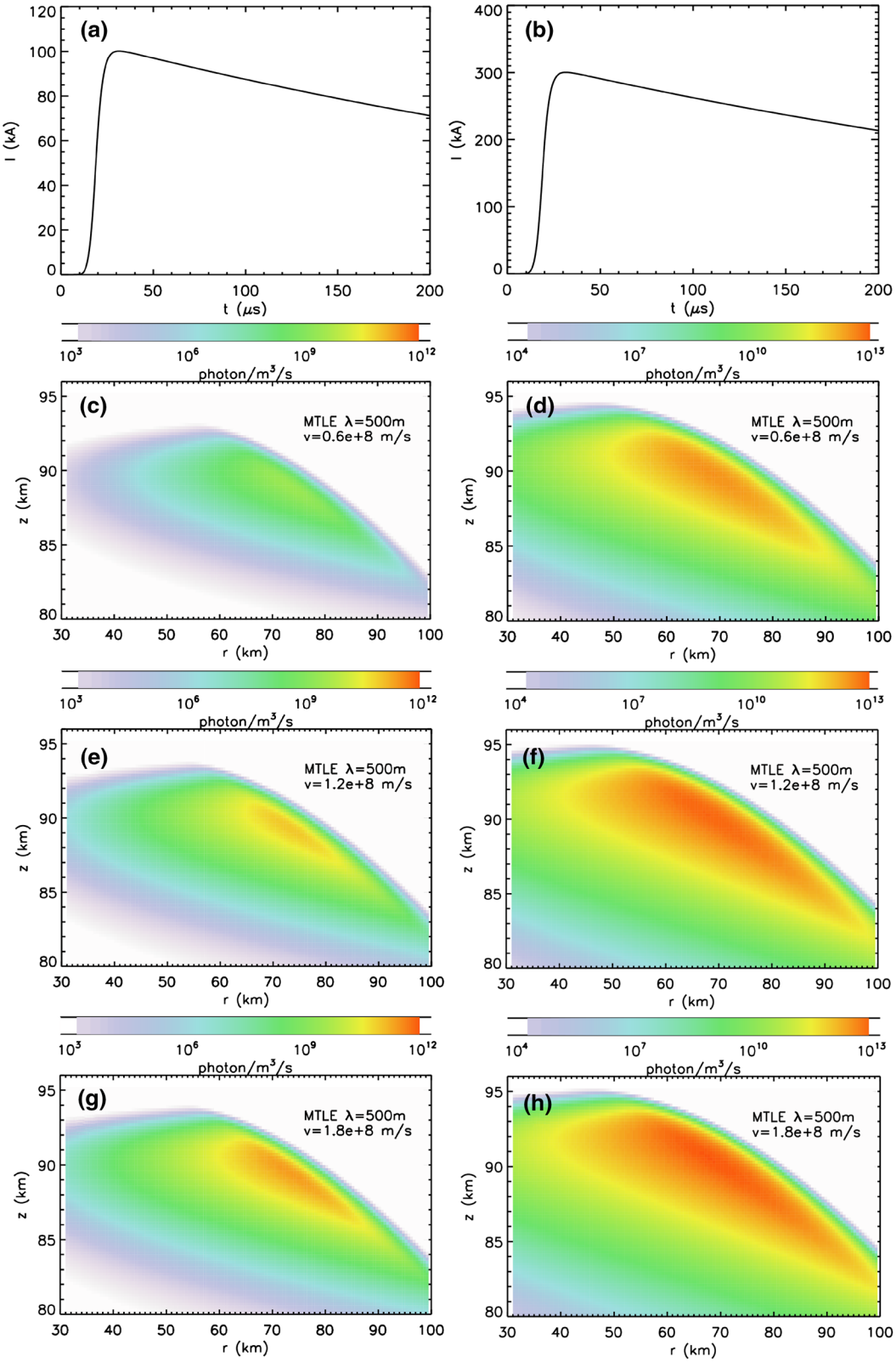

Figure 8. (a and b) Development of the channel base current with a maximum value of 100 kA and 300 kA, respectively; Production of photons per cubic meter per second for different return stroke current wave velocities (c and d) 20% of the speed of light, (e and f) 40% of the speed of light, and (g and h) 60% of the speed of light and a constant attenuation length $\lambda = 500$ m. Note that the color scales in the columns differ by one order of magnitude.

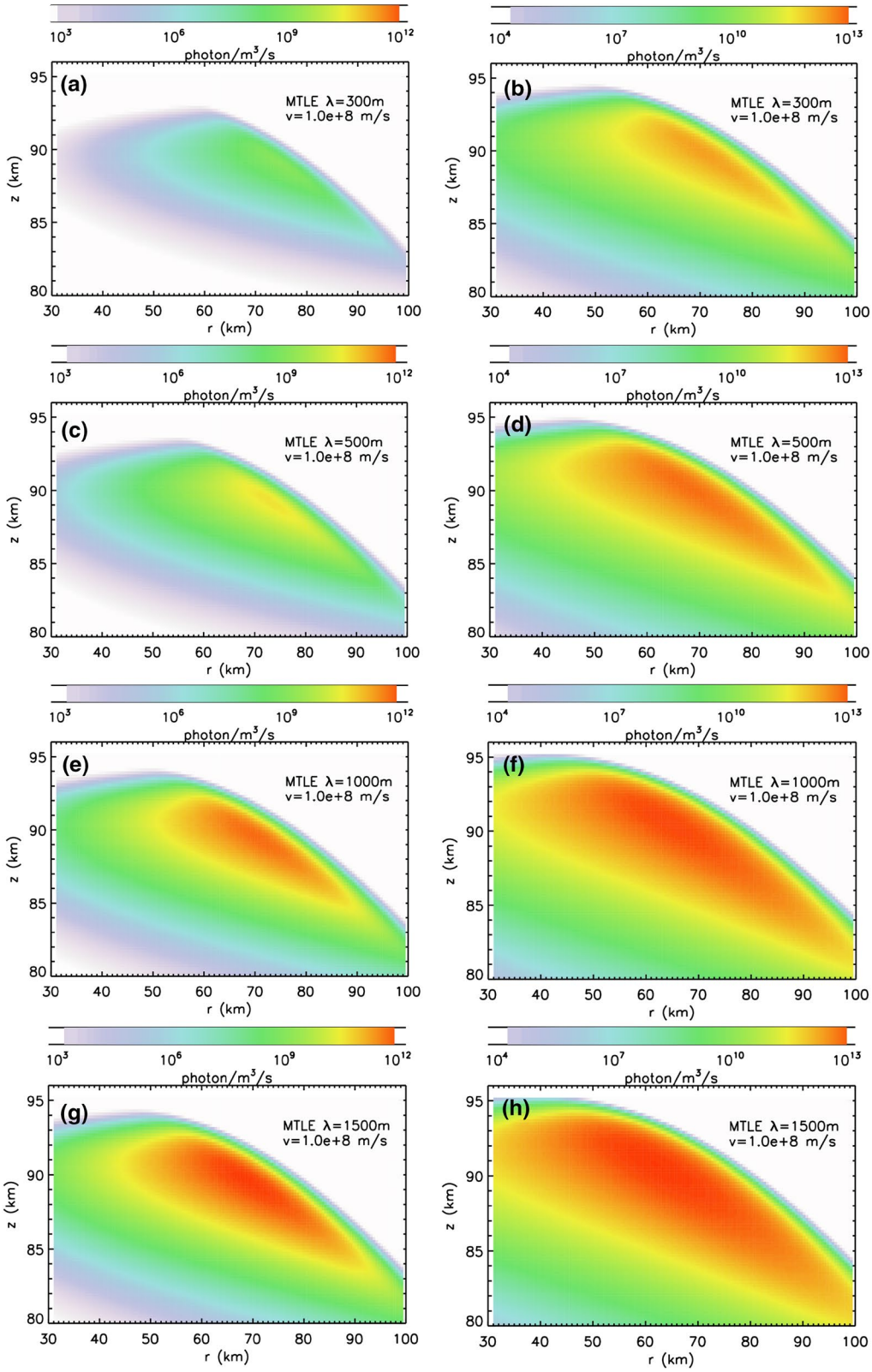

Figure 9. The number of photons per cubic meter per second for different attenuation lengths λ (a and b) 300 m, (c and d) 500 m, (e and f) 1,000 m, and (g and h) 1,500 m with a fixed RS peak current of 100 kA (a, c, e, and g) or 300 kA (b, d, f, and h) and a current wave velocity equal to one third of the speed of light. Note that the color scales in the columns differ by one order of magnitude.

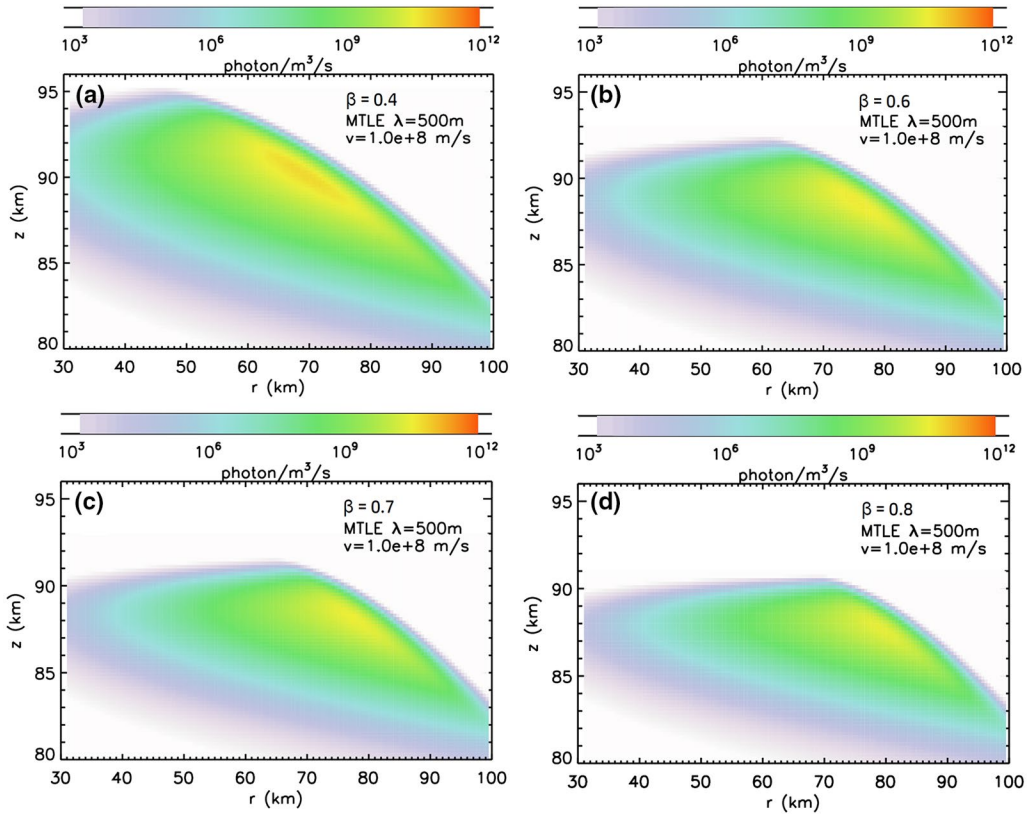

Figure 10. The number of photons per cubic meter per second for different values of the ionospheric steepness β (a) 0.4, (b) 0.6, (c) 0.7, and (d) 0.8 with a fixed RS peak current of 100 kA and a current wave velocity equal to one-third of the speed of light.

The variations in the length of the lightning channel did not influence the productions of photons as in the MTLE model with an exponential current decay with height the bottom part of the channel produces the highest contribution to the photon production. If we fix the peak current to 100 kA, the attenuation length to 1,500 m, the velocity of the current wave to one third of speed of light, and run our model for two different lengths of the lightning channel (3.5 and 7.5 km), the photon production reached in both cases the same maximum of 1.3×10^{12} photons/m^3/s. The difference in productions of photons excited by strokes with peak currents of 100 kA flowing in the 7.5 and 3.5 km long channels reached only 0.013‰.The ionosphere was rather turbulent during analyzed storm. The variations of the narrowband VLF signal (Figure 4b) indicate that both the electron density and its steepness β were not constant and that the initial ionospheric conditions for each captured elves were different. Therefore, we run our model for different values of β in order to evaluate the influence of its variations on the photon production. We keep the attenuation length equal to 500 m and the velocity of the current wave at one third of the speed of light as in Figure 9a, in which β is equal to 0.5. Then we have chosen all values of β derived from different measurements reported in the literature (Golkowski et al, 2018; A. Kumar & Kumar, 2020; S. Kumar et al., 2009; Thomson et al., 2007). The results for β equal to 0.4, 0.6, 0.7, and 0.8 are shown in Figure 10. It can be seen that steeper electron density profile leads to a decrease of the upper boundary of elves. At the same time, the region of the most intense production of photons is smaller and weaker and the apparent elves hole can be larger.

Cho and Rycroft (1998) showed that the amplitude and rise time of the return stroke current pulse influence the intensity of elves. We have demonstrated that the velocity of the current wave and the conductivity of the lightning channel of the causative lightning RS are other important factors that control the intensity of elves. Geographical and seasonal variations of conductivity could be expected since the highly conductive lightning plasma channel is maintained by Joule heating, but its dissipation is controlled by expansion and radiative cooling. Based on spectroscopic measurements of several lightning channels conducted in

different geographical conditions Guo et al. (2009) concluded that in China the conductivity of coastal RS lightning channels was higher than of those which hit the plateaus.

It is obvious that the conductivity of the lightning channel influences the amplitude of the RS pulse and that the velocity of the current wave is reflected in the rise time of the RS pulse. Unfortunately, we are not able to estimate these parameters reliably using our instrumentation. The cadence of the photometers (5 kHz) as well as the upper frequency limits of the VLF (25 and 39 kHz) and ELF (300 Hz) receivers are not sufficient to determine the velocity of the current waves from the rising times of the optical or electromagnetic RS pulses. We can only very roughly adjust the elves hole radii and estimate current wave velocities of causative RSs using the Figure 3a from Blaes et al. (2014): assuming a length of 7.5 km for the lightning channel we obtain about 40%, 50%, 70%, and 80% of the speed of light for E1, E2, E3, and E4, respectively.

6. Summary

A small-scale unusual continental spring-time thunderstorm (the first 2017 storm in Czechia) with a CAPE of 375 kJ/kg exceeding more than 3 times the usual April value, with an above-average afternoon temperature, and with winter-like cloud-tops of 9.5 km, was found to produce an extremely high fraction (55%) of positive CG RSs. Such a high percentage of CG+ lightning strokes is unusual even for winter thunderstorms. We can speculate that this high fraction of positive strokes might be a manifestation of the inverted polarity storm. Our model cannot rule out this charge arrangement. If we set a length of the lightning channel to 3.5 km, where we can expect the main positive charge center in case of an inverted polarity storm, the production of photons per cubic meter per second did not change substantially. The peak currents of detected positive strokes reached a mean of +93 kA (a median of +64 kA) while a mean peak current of negative RS was only 9 kA (a median of 5 kA). Four elves caused by exceptionally strong CG+ lightning strokes (>300 kA) were detected optically by a low-light camera at a distance of 430 km from the thunderstorm. These CG+ s occur in small but high radar reflectivity spots (Figure 1). These spots were probably rich reservoirs of the positive charge for such strong CG+, similarly as in Japan (Takahashi et al., 2003) or Mediterranean (Ganot et al., 2007).

Independent signatures of horizontal ionospheric disturbances indicate a presence of elves in agreement with records of displacement currents at ~1,100 km distance from the storm and also in electromagnetic VLF measurements of ionospherically reflected sferics recorded 800 and 2,100 km from the storm. The peaks in the covariance plots calculated from measurements of displacement currents indicate the presence of extensive horizontal ionospheric electron density enhancement and can be without any ambiguity for the first time assigned to elves-producing strokes. Large changes of the electron density in the lower ionosphere that lead to changes in the reflection efficiency for narrow-band VLF signals close to the elve locations were also confirmed by detection of LOREs in the measurements of the signal intensity of the DHO38 transmitter. As the distance between the signal propagation path and the thunderstorm location was about 300 km, detection of LOREs imply peak currents of causative strokes larger than 250 kA (Haldoupis et al., 2013).

All these electromagnetic observations, which are not dependent on the sensitivity of the camera or on the background luminosity level of the night sky, coincide with the four optically detected elves and indirectly indicate the presence of two other elves that occur later in the decaying phase of the storm. Surprisingly, the same electromagnetic measurements indicate that other strong strokes (20 strokes above 100 kA) were not producing observable elves. At the same time, ELF magnetic field and fast photometer measurements of RS did not indicate conditions allowing or preventing the occurrence of elves. The optical properties of elves and electromagnetic properties of their causative RSs, including the optically undetected elves are summarized in Table 1. The table contains also optical and electromagnetic properties of all strong strokes detected in Rustrel. The table clearly shows that the relation of the peak currents of elve-parent strokes with optical properties of elves, current moments or charge moment changes of their causative RSs is very weak or is missing at all. It supports our assumption that there are also other properties of RSs, which control generation of elves. We simulated optical emissions in the lower ionosphere associated with high peak current lightning strokes. Our model is based on the transmission line model with an attenuation of the current with height. We run our model for numerous combinations of different parameters, which might influence the production of the optical emissions. For two peak currents of causative strokes (100 and 300 kA) we

have varied the velocity of the RS current waves, the ionospheric sharpness, the length of the lightning channel and its conductivity represented by the attenuation length.

We show by means of modeling that the formation of elves is not only determined by the high-peak currents of their causative strokes but that it is also controlled by the conductivity of the lightning channels, velocities of the current wavefronts, and by the sharpness of the ionosphere. In summary, we hypothesize that less conductive RS lightning channels and/or slower current waves flowing in these channels might have been associated with the unusual small-scale continental spring-time thunderstorm described in this study. We also cannot rule out that the electron density profile of the lower ionosphere above the thunderstorm was not very sharp. As a result, only extremely strong lightning strokes with peak currents exceeding 300 kA might have been capable to produce observable elves in this specific case.

Data Availability Statement

All other data are available at http://dx.doi.org/10.17632/z5y3ggw6gm.1. Rustrel VLF data are available at http://bleska.ufa.cas.cz/lsbb/storage/elm/.

Acknowledgment
The work of I. Kolmašová and O. Santolík was supported by European Regional Development Fund-Project CRREAT (CZ.02.1.01/0.0/0.0/15_003 /0000481) and by the Praemium Academiae award of the Czech Academy of Sciences. The work of P. Kašpar, M. Popek, R. Lán, and L. Uhlíř was supported by the GACR grant 20-09671S. Similarly, another Preamium Academiae award of the CAS supported the work of P. Spurný and J. Borovička. The above listed authors thanks the Strategy AV21 of the Czech Academy of Sciences for valuable support. The National Science Center, Poland, under grant 2015/19/B/ ST10/01055, supported the work of J. Mlynarczyk. We thank Laboratoire Souterrain à Bas Bruit, UNS/UAPV/ CNRS, Rustrel, France, and its Director S. Gaffet, for hosting our VLF receiving station at their facility at La Grande Montagne.

References

Barrington-Leigh, C. P., & Inan, U. S. (1999). Elves triggered by positive and negative lightning discharges. *Geophysical Research Letters*, *26*(6), 683–686. https://doi.org/10.1029/1999GL900059

Ben Ami, Y., Altaratz, O., Yair, Y., & Koren, I. (2015). Lightning characteristics over the eastern coast of the Mediterranean during different synoptic systems. *Natural Hazards and Earth System Sciences*, *15*(11), 2449–2459. https://doi.org/10.5194/nhess-15-2449-2015

Bennett, A. J. (2013). Identification and ranging of lightning flashes using co-located antennas of different geometry. *Measurement Science and Technology*, *24*(12), 8. https://doi.org/10.1088/0957-0233/24/12/125801

Bennett, A. J. (2014). Modification of lightning quasi-electrostatic signal by mesospheric halo generation. *Journal of Atmospheric and Solar-Terrestrial Physics*, *113*, 39–43. https://doi.org/10.1016/j.jastp.2014.03.010

Bennett, A. J. (2017). Electrostatic thunderstorm detection. *Weather*, *72*, 51–54. https://doi.org/10.1002/wea.2927

Bennett, A. J., & Harrison, R. G. (2013). Lightning-induced extensive charge sheets provide long range electrostatic thunderstorm detection. *Physical Review Letters*, *111*(4), 045003. https://doi.org/10.1103/PhysRevLett.111.045003

Blaes, P. R., Marshall, R. A., & Inan, U. S. (2014). Return stroke speed of cloud-to-ground lightning estimated from elve hole radii. *Geophysical Research Letters*, *41*(24), 9182–9187. https://doi.org/10.1002/2014GL062392

Blaes, P. R., Marshall, R. A., & Inan, U. S. (2016). Global occurrence rate of elves and ionospheric heating due to cloud-to-ground lightning. *Journal of Geophysical Research: Space Physics*, *121*(1), 699–712. https://doi.org/10.1002/2015JA021916

Chen, A. B., Kuo, C.-L., Lee, Y.-J., Su, H.-T., Hsu, R.-R., Chern, J.-L., et al. (2008). Global distributions and occurrence rates of transient luminous events. *Journal of Geophysical Research*, *113*, A08306. https://doi.org/10.1029/2008JA013101

Chen, A. B. C., Su, H.-T., & Hsu, R.-R. (2014). Energetics and geographic distribution of elve-producing discharges. *Journal of Geophysical Research: Space Physics*, *119*(2), 1381–1391. https://doi.org/10.1002/2013JA019470

Cho, M., & Rycroft, M. J. (1998). Computer simulation of the electric field structure and optical emission from cloud-top to the ionosphere. *Journal of Atmospheric and Solar-Terrestrial Physics*, *60*(7–9), 871–888. https://doi.org/10.1016/S1364-6826(98)00017-0

Cummer, S. A. (2003). Current moment in sprite-producing lightning. *Journal of Atmospheric and Solar-Terrestrial Physics*, *65*(5), 499–508. https://doi.org/10.1016/S1364-6826(02)00318-8

Cummins, K. L. (2000). Continental-scale detection of cloud-to-ground lightning. *IEEJ Transactions on Power and Energy*, *120*(1), 2–5.

Farges, T., Blanc, E., & Tanguy, M. (2007). Experimental evidence of D region heating by lightning-induced electromagnetic pulses on MF radio links. *Journal of Geophysical Research*, *112*, A10302. https://doi.org/10.1029/2007JA012285

Fukunishi, H., Takahashi, Y., Kubota, M., Sakanoi, K., Inan, U., & Lyons, W. (1996). Elves: Lightning-induced transient luminous events in the lower ionosphere. *Geophysical Research Letters*, *23*(16), 2157–2160. https://doi.org/10.1029/96GL01979

Füllekrug, M., Kolmasova, I., Santolik, O., Farges, T., Bor, J., Bennett, A., et al. (2013). Electron acceleration above thunderclouds. *Environmental Research Letters*, *8*(3), 035027. https://doi.org/10.1088/1748-9326/8/3/035027

Ganot, M., Yair, Y., Price, C., Ziv, B., Sherez, Y., Greenberg, E., et al. (2007). First detection of transient luminous events associated with winter thunderstorms in the eastern Mediterranean. *Geophysical Research Letters*, *34*, L12801. https://doi.org/10.1029/2007GL029258

Gołkowski, M., Sarker, S. R., Renick, C., Moore, R. C., Cohen, M. B., Kułak, A., et al. (2018). Ionospheric D region remote sensing using ELF sferic group velocity. *Geophysical Research Letters*, *45*. https://doi.org/10.1029/2018GL080108

Greenberg, E., Price, C., Yair, Y., Ganot, M., Bór, J., & Sátori, G. (2007). ELF transients associated with sprites and elves in eastern Mediterranean winter thunderstorms. *Journal of Atmospheric and Solar-Terrestrial Physics*, *69*(13), 1569–1586. https://doi.org/10.1016/j.jastp.2007.06.002

Guo, Y.-X., Yuan, P., Shen, X.-Z., & Wang, J. (2009). The electrical conductivity of a cloud-to-ground lightning discharge channel. *Physica Scripta*, *80*(3), 035901. https://doi.org/10.1088/0031-8949/80/03/035901

Haldoupis, C., Cohen, M., Arnone, E., Cotts, B., & Dietrich, S. (2013). The VLF fingerprint of elves: Step-like and long-recovery early VLF perturbations caused by powerful ±CG lightning EM pulses. *Journal of Geophysical Research: Space Physics*, *118*, 5392–5402. https://doi.org/10.1002/jgra.50489

Haldoupis, C., Neubert, T., Inan, U. S., Mika, A., Allin, T. H., & Marshall, R. A. (2004). Subionospheric early VLF signal perturbations observed in one-to one association with sprites. *Journal of Geophysical Research*, *109*, A10303. https://doi.org/10.1029/2004JA010651

Hedin, A. E. (1991). Extension of the MSIS thermosphere model into the middle and lower atmosphere. *Journal of Geophysical Research*, *96*(A2), 1159–1172. https://doi.org/10.1029/90JA02125

Heidler, F., & Cvetić, J. (2002). A class of analytical functions to study the lightning effects associated with the current front. *European Transactions on Electrical Power*, *12*(2), 141–150. https://doi.org/10.1002/etep.4450120209

Hobara, Y., Iwasaki, N., Hayashida, T., Hayakawa, M., Ohta, K., & Fukunishi, H. (2001). Interrelation between ELF transients and ionospheric disturbances in association with sprites and elves. *Geophysical Research Letters*, *28*(5), 935–938. https://doi.org/10.1029/2000GL003795

Holzworth, R. H., McCarthy, M. P., Brundell, J. B., Jacobson, A. R., & Rodger, C. J. (2019). Global distribution of superbolts. *Journal of Geophysical Research: Atmospheres*, *124*, 9996–10005. https://doi.org/10.1029/2019JD030975

Huang, E., Williams, E., Boldi, R., Heckman, S., Lyons, W., Taylor, M., et al. (1999). Criteria for sprites and elves based on Schumann resonance observations. *Journal of Geophysical Research*, *104*(D14), 16943–16964. https://doi.org/10.1029/1999JD900139

Inan, U. S., Barrington-Leigh, C. P., Hansen, S., Glukhov, V. S., Bell, T. F., & Rairden, R. (1997). Rapid lateral expansion of optical luminosity in lightning-induced ionospheric flashes referred to as 'elves'. *Geophysical Research Letters*, *24*(5), 583–586. https://doi.org/10.1029/97GL00404

Inan, U. S., Bell, T. F., & Rodriguez, J. V. (1991). Heating and ionization of the lower ionosphere by lightning. *Geophysical Research Letters*, *18*(4), 705–708. https://doi.org/10.1029/91GL00364

Inan, U. S., Cummer, S. A., & Marshall, R. A. (2010). A survey of ELF and VLF research on lightning-ionosphere interactions and causative discharges. *Journal of Geophysical Research*, *115*(A6), A00E36. https://doi.org/10.1029/2009JA014775

Inan, U. S., Sampson, W. A., & Taranenko, Y. N. (1996). Space-time structure of optical flashes and ionization changes produced by lightning-EMP. *Geophysical Research Letters*, *23*(2), 133–136. https://doi.org/10.1029/95GL03816

Kulak, A., Kubisz, J., Klucjasz, S., Michalec, A., Mlynarczyk, J., Nieckarz, Z., et al. (2014). Extremely low frequency electromagnetic field measurements at the Hylaty station and methodology of signal analysis. *Radio Science*, *49*(6), 361–370. https://doi.org/10.1002/2014RS005400

Kulak, A., & Mlynarczyk, J. (2013). ELF propagation parameters for the ground-ionosphere waveguide with finite ground conductivity. *IEEE Transactions on Antennas and Propagation*, *61*(4), 2269–2275. https://doi.org/10.1109/TAP.2012.2227445

Kumar, S., Deo, A., & Ramachandran, V. (2009). Nighttime D-region equivalent electron density determined from tweek sferics observed in the South Pacific Region. *Earth Planets and Space*, *61*, 905–911.

Kumar, A., & Kumar, S. (2020). Ionospheric D region parameters obtained using VLF measurements in the South Pacific region. *Journal of Geophysical Research: Space Physics*, *125*, e2019JA027536. https://doi.org/10.1029/2019JA027536

Kuo, C. L., Chen, A. B., Lee, Y. J., Tsai, L. Y., Chou, R. K., Hsu, R. R., et al. (2007). Modeling elves observed by FORMOSAT-2 satellite. *Journal of Geophysical Research*, *112*(A11), A11312. https://doi.org/10.1029/2007JA012407

Kuo, C. L., Huang, T.-Y., Chang, S. C., Chou, J. K., Lee, L. J., Wu, Y. J., et al. (2012). Full-kinetic elve model simulations and their comparisons with the ISUAL observed events. *Journal of Geophysical Research: Space Physics*, *117*, A07320. https://doi.org/10.1029/2012JA017599

Liu, N. Y., Dwyer, J. R., & Cummer, S. A. (2017). Elves accompanying terrestrial gamma ray flashes. *Journal of Geophysical Research: Space Physics*, *122*, 10563–10576. https://doi.org/10.1002/2017JA024344

MacGorman, D., Rust, W. D., Krehbiel, P., Rison, W., Bruning, E., & Wiens, K. (2005). The electrical structure of two supercell storms during STEPS. *Monthly Weather Review*, *133*(9), 2583–2607. https://doi.org/10.1175/MWR2994.1

Mach, D. M., & Rust, W. D. (1993). Two-dimensional velocity, optical risetime, and peak current estimates for natural positive lightning return strokes. *Journal of Geophysical Research*, *98*(D2), 2635–2638.

Manninen, J., Turunen, T., Kleimenova, N., Rycroft, M., Gromova, L., & Sirviö, I. (2016). Unusually high frequency natural VLF radio emissions observed during daytime in Northern Finland. *Environmental Research Letters*, *11*(12), 1–8. https://doi.org/10.1088/1748-9326/11/12/124006

Market, P. S., & Becker, A. E. (2009). A study of lightning flashes attending periods of banded snowfall. *Geophysical Research Letters*, *36*(1), L01809. https://doi.org/10.1029/2008GL036317

Marshall, R. A., Inan, U. S., & Glukhov, V. S. (2010). Elves and associated electron density changes due to cloud-to-ground and in-cloud lightning discharges. *Journal of Geophysical Research*, *115*(A4), A00E17. https://doi.org/10.1029/2009JA014469

Marshall, R. A., Silva, C. L., & Pasko, V. P. (2015). Elve doublets and compact intracloud discharges. *Geophysical Research Letters*, *42*(14), 6112–6119. https://doi.org/10.1002/2015GL064862

Mika, A., Haldoupis, C., Neubert, T., Su, R. R., Hsu, H. T., Steiner, R. J., & Marshall, R. A. (2006). Early VLF perturbations observed in association with elves. *Annales Geophysicae*, *24*, 2179–2189. https://doi.org/10.5194/angeo-24-2179-2006

Mlynarczyk, J., Bór, J., Kulak, A., Popek, M., & Kubisz, J. (2015). An unusual sequence of sprites followed by a secondary TLE: An analysis of ELF radio measurements and optical observations. *Journal of Geophysical Research: Space Physics*, *120*(3), 2241–2254. https://doi.org/10.1002/2014JA020780

Montanyà, J., van der Velde, O., Romero, D., March, V., Solà, G., Pineda, N., et al. (2010). High-speed intensified video recordings of sprites and elves over the western Mediterranean Sea during winter thunderstorms. *Journal of Geophysical Research*, *115*(A4), A00E18. https://doi.org/10.1029/2009JA014508

Moudry, D., Stenbaek-Nielsen, H., Sentman, D., & Wescott, E. (2003). Imaging of elves, halos and sprite initiation at 1 ms time resolution. *Journal of Atmospheric and Solar-Terrestrial Physics*, *65*(5), 509–518. https://doi.org/10.1016/S1364-6826(02)00323-1

Mussa, R., for the Pierre Auger Collaboration (2019). Analysis of elves at the Pierre Auger Observatory. *EPJ Web of Conferences*, *197*, 03004. https://doi.org/10.1051/epjconf/201919703004

Neubert, T., Østgaard, N., Reglero, V., Chanrion, O., Heumesser, M., Dimitriadou, K., et al. (2019). A terrestrial gamma-ray flash and ionospheric ultraviolet emissions powered by lightning. *Science*, *367*(6474), 183–186. https://doi.org/10.1126/science.aax3872

Newsome, R. T., & Inan, U. S. (2010). Free-running ground-based photometric array imaging of transient luminous events. *Journal of Geophysical Research*, *115*(A7), A00E41. https://doi.org/10.1029/2009JA014834

Novák, P. (2007). The Czech Hydrometeorological Institute's severe storm nowcasting system. *Atmospheric Research*, *83*(2–4), 450–457. https://doi.org/10.1016/j.atmosres.2005.09.014

Novak, P., & Kyznarova, H. (2011). Climatology of lightning in the Czech Republic. *Atmospheric Research*, *100*, 318–333. https://doi.org/10.1016/j.atmosres.2010.08.022

Pérez-Invernón, F. J., Luque, A., & Gordillo-Vázquez, F. J. (2018a). Modelling the chemical impact and the optical emissions produced by lightning-induced electromagnetic fields in the upper atmosphere: The case of halos and elves triggered by different lightning discharges. *Journal of Geophysical Research: Atmospheres*, *123*(14), 7615–7641. https://doi.org/10.1029/2017JD028235

Pérez-Invernón, F. J., Luque, A., Gordillo-Vázquez, F. J., Sato, M., Ushio, T., Adachi, T., & Chen, A. B. (2018b). Spectroscopic diagnostic of halos and elves detected from space-based photometers. *Journal of Geophysical Research: Atmospheres*, *123*(22), 12917–12941. https://doi.org/10.1029/2018JD029053

Poelman, D. R., Schulz, W., Diendorfer, G., & Bernardi, M. (2016). The European lightning location system EUCLID – Part 2: Observations. *Natural Hazards and Earth System Sciences*, *16*, 607–616. https://doi.org/10.5194/nhess-16-607-2016

Rakov, V. A., & Uman, M. A. (1998). Review and evaluation of lightning return stroke models including some aspects of their application. *IEEE Transactions on Electromagnetic Compatibility*, *40*(4), 403–426. https://doi.org/10.1109/15.736202

Santolík, O., & Kolmašová, I. (2017). Unusual electromagnetic signatures of European North Atlantic winter thunderstorms. *Scientific Reports*, *7*, 13948. https://doi.org/10.1038/s41598-017-13849-4

Schulz, W., Diendorfer, G., Pedeboy, S., & Poelman, D. R. (2016). The European lightning location system EUCLID – Part 1: Performance analysis and validation. *Natural Hazards and Earth System Sciences*, *16*, 595–605. https://doi.org/10.5194/nhess-16-595-2016

Schulz, W., Pedeboy, S., & Poelman, D. R. (2014). Performance validation of the European lightning location system EUCLID. *Conference paper in Natural Hazards and Earth System Sciences Discussions-May 2014*. https://doi.org/10.5194/nhessd-3-5325-2015

Soula, S., van der Velde, O., Montanya, J., Neubert, T., Chanrion, O., & Ganot, M. (2009). Analysis of thunderstorm and lightning activity associated with sprites observed during the EuroSprite campaigns: Two case studies. *Atmospheric Research*, *91*(2–4), 514–528. https://doi.org/10.1016/j.atmosres.2008.06.017

Spurný, P., Borovička, J., Mucke, H., & Svoreň, J. (2017). Discovery of a new branch of the Taurid meteoroid stream as a real source of potentially hazardous bodies. *Astronomy & Astrophysics*, *605*, A68. https://doi.org/10.1051/0004-6361/201730787

Stolzenburg, M., & Marshall, T. C. (2008). Charge structure and dynamics in thunderstorms. *Space Science Reviews*, *137*, 355–372. https://doi.org/10.1007/s11214-008-9338-z

Suzuki, T., Matsudo, Y., Asano, T., Hayakawa, M., & Michimoto, K. (2011). Meteorological and electrical aspects of several winter thunderstorms with sprites in the Hokuriku area of Japan. *Journal of Geophysical Research*, *116*(D6), D06205. https://doi.org/10.1029/2009JD013358

Takahashi, Y., Miyasato, R., Adachi, T., Adachi, K., Sera, M., Uchida, A., & Fukunishi, H. (2003). Activities of sprites and elves in the winter season, Japan. *Journal of Atmospheric and Solar-Terrestrial Physics*, *65*(5), 551–560. https://doi.org/10.1016/S1364-6826(02)00330-9

Taranenko, Y. N., Inan, U. S., & Bell, T. F. (1993). The interaction with the lower ionosphere of electromagnetic pulses from lightning: Heating, attachment, and ionization. *Geophysical Research Letters*, *20*(15), 1539–1542. https://doi.org/10.1029/93GL01696

Taszarek, M., Brooks, H. E., Czernecki, B., Szuster, P., & Fortuniak, K. (2018). Climatological aspects of convective parameters over Europe: A comparison of ERA-interim and sounding data. *Journal of Climate*, *31*, 4281–4308.

Thomson, N. R., Clilverd, M. A., & McRae, W. M. (2007). Nighttime ionospheric D region parameters from VLF phase and amplitude. *Journal of Geophysical Research*, *112*, A07304. https://doi.org/10.1029/2007JA012271

Uman, M. A., McLain, D. K., & Krider, E. P. (1975). The electromagnetic radiation from a finite antenna. *American Journal of Physics*, *43*(1), 33–38.

van der Velde, O. A., & Montanyà, J. (2016). Statistics and variability of the altitude of elves. *Geophysical Research Letters*, *43*, 5467–5474. https://doi.org/10.1002/2016GL068719

van der Velde, O. A., Montanyà, J., Füllekrug, M., & Soula, S. (2011). Gravity waves, meteor trails and asymmetries in elves. *Paper presented at 14th International Conference on Atmospheric Electricity, August 08-12*. Rio de Janeiro, Brazil.

Veronis, G., Pasko, V. P., & Inan, U. S. (1999). Characteristics of mesospheric optical emissions produced by lightning discharges. *Journal of Geophysical Research*, *104*(A6), 12645–12656. https://doi.org/10.1029/1999JA900129

Wilcox, L. J., Hoskins, B. J., & Shine, K. P. (2012). A global blended tropopause based on ERA data. Part I: Climatology. *Quarterly Journal of the Royal Meteorological Society*, *138*, 561–575.

Wu, T., Yoshida, S., Ushio, T., Kawasaki, Z., Takayanagi, Y., & Wang, D. (2014). Large bipolar lightning discharge events in winter thunderstorms in Japan. *Journal of Geophysical Research*, *119*(2), 555–566. https://doi.org/10.1002/2013JD020369

Yair, Y., Price, C., Ganot, M., Greenberg, E., Yaniv, R., Ziv, B., et al. (2009). Optical observations of transient luminous events associated with winter thunderstorms near the coast of Israel. *Atmospheric Research*, *91*(2–4), 529–537. https://doi.org/10.1016/j.atmosres.2008.06.018

Yue, J., & Lyons, W. A. (2015). Structured elves: Modulation by convectively generated gravity waves. *Geophysical Research Letters*, *42*, 1004–1011. https://doi.org/10.1002/2014GL062612

Zhang, M., Yuana, P., Liu, G., Wang, X., Cen, J., & An, T. (2019). The current variation along the discharge channel in cloud-to-ground lightning. *Atmospheric Research*, *225*, 121–130. https://doi.org/10.1016/j.atmosres.2019.04.001